

Data Descriptor

Full-Density Fused Deposition Modeling Dimensional Error as a Function of Raster Angle and Build Orientation: Large Dataset for Eleven Materials

Sherri L. Messimer¹, Tais Rocha Pereira^{1,2}, Albert E. Patterson^{1,3,*} , Maliha Lubna¹, and Fabiano O. Drozda²

¹ Department of Industrial & Systems Engineering and Engineering Management, University of Alabama in Huntsville, Technology Hall N143, 300 Sparkman Drive, Huntsville, Alabama, 35899, USA: taisrocha@ufpr.br (T.R.P.); maliha.lubna@uah.edu (M.L.); sherri.messimer@uah.edu (S.L.M.)

² Department of Production Engineering, Federal University of Paraná, Rue XV de Novembro, 1299-Centro, Curitiba 80060-000, Brazil; fabiano.drozda@ufpr.br

³ Department of Industrial and Enterprise Systems Engineering, University of Illinois at Urbana-Champaign, 117 Transportation Building, 104 South Mathews Avenue, Urbana, IL 61801, USA

* Correspondence: ptttrsnv2@illinois.edu; Tel.: +1-217-333-2731

Abstract: This report describes the collection of a large dataset (6930 measurement) on dimensional error in the fused deposition modeling (FDM) additive manufacturing process for full-density parts. Three different print orientations were studied, as well as seven raster angles (0°, 15°, 30°, 45°, 60°, 75°, and 90°) for the rectilinear infill pattern. All measurements were replicated ten times on ten different samples to ensure a comprehensive dataset. Eleven polymer materials were considered: acrylonitrile butadiene styrene (ABS), polylactic acid (PLA), high-temperature PLA, wood-composite PLA, carbon-fiber-composite PLA, copper-composite PLA, aluminum-composite PLA, high-impact polystyrene (HIPS), polyethylene terephthalate glycol-enhanced (PETG), polycarbonate, and synthetic polyamide (nylon). The samples were ASTM-standard impact testing samples, since this geometry allows the measurement of error on three different scales; the nominal dimensions were 3.25mm thick, 63.5mm long, and 12.7mm wide. This dataset is intended to give engineers and product designers a benchmark for judging the accuracy and repeatability of the FDM process for use in manufacturing of end-user products.

Dataset: Attached with manuscript

Dataset License: CC-BY

Keywords: Additive manufacturing; fused deposition modeling; FDM; dimensional accuracy; manufacturing process repeatability; polymer testing

1. Summary

As additive manufacturing (AM) technologies becomes more widely used for manufacturing, it is increasingly necessary to consider their impact on engineering design methods. In contrast with more traditional subtractive and formative processes, AM produces geometry by depositing the raw material in layers and fusing those layers together using some mechanism (typically heat or chemical reaction) [1–3]. There are a wide variety of processes available, divided roughly into seven families [2,3] based on the state of the raw material, the method of producing layers, and the method of layer fusion. There are many benefits to using AM processes in manufacturing of end-user parts, including the ability to produce extremely complex geometry directly from digital models [4,5] and the freedom from formal tooling requirements [6,7]. Various AM methods can process a wide variety of polymer, metal, and ceramic materials; some hybrid processes have recently emerged [8–12] which can use more than one class of material in the same part and process.

However, there are some limitations and problems that need to be considered and addressed when using AM, dimensional accuracy [13,14], process and geometric repeatability [15–17], and material defects [18–20] being the primary considerations. While all of these are important to examine, the most important from the perspective of engineering design are the dimensional accuracy and repeatability of the final parts. It has been observed that most of the problems with the dimensional accuracy in AM are due to the material behavior [13,21–23] and to the limitations and mechanics of the processing equipment [24–26]. Since most AM processes involve heating the material past the glass transition temperature, shrinkage of the material is a concern; this shrinkage can both destroy the dimensional integrity of the part and introduce residual stresses, potentially reducing the material fatigue life as well. Vibration and mechanical compliance are the primary sources of error from the processing equipment, but the effects of this vary significantly from process-to-process.

One of the most common and important AM processes for processing polymer and polymer-composite materials is the extrusion-based Fused Deposition Modeling (FDM) process. Originally developed primarily as a simple prototyping process, it has seen much development in recent years and has become suited for manufacturing of end-user products in some industries. FDM works by selectively extruding a bead or molten or near-molten material to build up the part in layers (Figure 1). The raw material is put into the machine in the form of a filament, the layering is done via the deposition from the extruder, and the fusion is done by chemical reaction as the deposited material cools onto the previous layer [27–32].

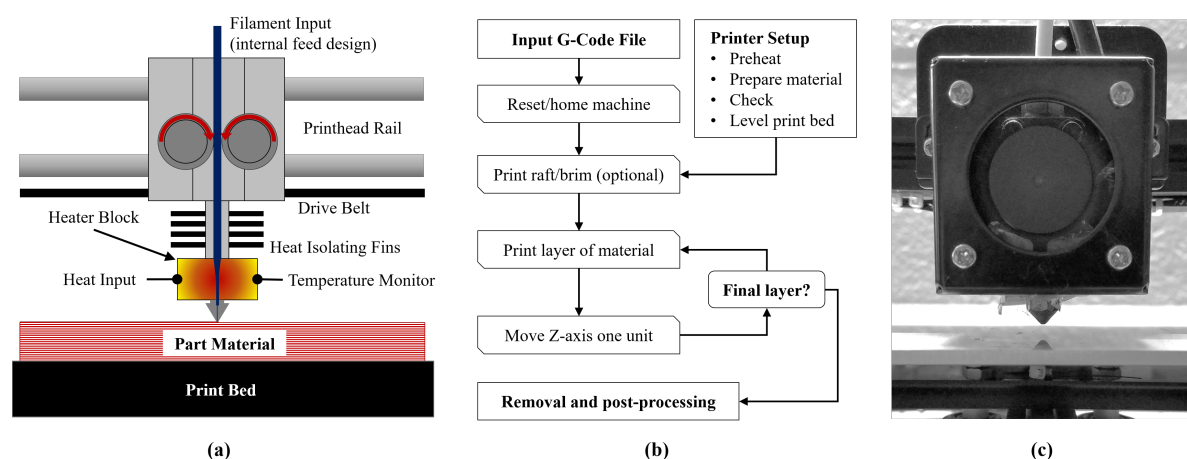


Figure 1. Fused deposition modeling (FDM) (a) process diagram, (b) work-flow, and (c) extruder carriage example [27]

Due to the mechanics of the process, FDM is potentially subject to several sources of error from vibration and mechanical compliance. This can be mitigated somewhat by ensuring that the machine is in good mechanical condition, with good-quality timing belts and bearings, and by using control settings which reduce the effect of vibration. One of the most important parameters which is often not discussed in the current literature is the effect of the jerk setting; the *jerk* is defined as the minimal difference (typically expressed in mm/s) between a current and desired printhead velocity for which the drive motor (typically a stepper motor) will ramp up its torque instead of applying it all at once. Below this setting, the motor will apply torque fully, causing the printhead to “jerk” into the desired position. A high jerk setting ($> 20\text{ mm/s}$ in the experience of the authors) will increase the print speed significantly, but will also cause the printhead to snap and overshoot during processing, introducing errors. Conversely, a very low jerk setting ($< 1\text{ mm/s}$) will prevent the printhead from moving smoothly and may cause problems with the melt-pool of the extruded material since the material will extrude very slowly. After extensive experimentation, the authors have found that an average jerk setting of 8 mm/s provided a good balance and therefore was used to produce the samples in this

study. The actual optimization of this parameter has not yet been explored in-depth in the literature, but is something that should be examined further in future work.

It was observed that a dimensional error as low as 0.15% could be accomplished for FDM with the correct settings [13,33–40], but this is highly dependent on the size of the samples in question; smaller samples showed a much higher error. In terms of raw dimensional error, most studies showed the capability to build parts with an error under $200\mu\text{m}$ regardless of the specimen size. While most studies reported the error as a percentage of the sample dimensions, it is clear from the data presented that the error is related more to the raw dimensions, and so different sample sizes will show different percentage errors for the same material and parameters.

To further study the aspects of FDM dimensional accuracy and repeatability, a large dataset of observed dimensional errors for various materials and printing parameters was collected using a large number of relatively simple identical parts; the summary, major considerations, and the collection procedure are discussed in the proceedings sections. This dataset is intended to assist designers and process engineers in evaluating the feasibility of FDM as an end-product manufacturing process. Interpretation of the data was not part of this study, as this work focused on collecting useful data which can be used to guide the solutions to a wide variety of design and manufacturing problems. A number of factors were considered for their influence on the two main variables for a large number of materials, so this dataset can be used to study correlations between the parameters, the material properties, and accuracy/repeatability of FDM. Each datapoint was repeated ten times, so reliable values of the sample mean and variance can be found easily, allowing the calculation of probability distributions for sections of the dataset. This data will also be useful as a training input for finite element analyses, for optimization algorithms, and for machining learning processes that evaluate FDM.

2. Data Description

2.1. Overview and Experiment Considerations

Previous FDM dimensional accuracy studies and design approaches [13,27–40] have mainly focused on establishing the dimensional integrity of complex features; these are very useful studies for predicting the accuracy relative to process parameters and for one-off complex parts. However, as FDM begins to be a viable option for end-product manufacturing, a large dataset derived from relatively simple specimens is needed, one that can be used for statistical analysis in order to determine the expected accuracy and repeatability over a large number of parts. Such a dataset could be especially useful in the establishment of tolerance constraints on parts during design, as well as finding correlations between the basic process parameters and the accuracy/repeatability. A subset of the possible process parameters can be considered (the exact values of these parameters are given in Section 3) most important for the study presented in this report:

- **Print Orientation:** Print orientations corresponding to the three Cartesian axes were used
- **Density:** All parts were printed full-density (100% infill) for all materials; all gaps in the mesostructure were set to zero in the processing gcode for the samples.
- **Infill pattern:** A standard rectilinear infill pattern was used
- **Print velocity:** Printing velocity was set at a standard value, unless a lower setting was necessitated by material behavior
- **Jerk:** The print jerk was fixed at the same value for all specimens and materials
- **Processing temperatures:** Appropriate extruder and build plate temperatures were used for each of the materials
- **Nozzle:** Some materials were printed using standard brass nozzles, but others required one made from tool steel; all nozzles used were identical in size

- **Enclosure:** Some materials that were sensitive to warping, emitted odors, or were sensitive to humidity were printed inside of an enclosure, while the rest were printed on a standard open-bed machine in a conditioned environment
- **Layer resolution:** All samples for all materials used the same layer resolution
- **Bed interface:** All samples were printed using rafts on heated glass or polycarbonate build plates, as appropriate for the material
- **Experimental environment:** All samples were manufactured and tested in a climate-controlled environment at least 40 hours before measuring, as recommended by several ASTM standards for testing polymeric materials

Even though eleven different materials were used in this study, the difference in material was not considered to be an experimental factor; different materials required different printing parameters and had different reactions on cooling after the processing. Some materials were very stable and some were not; the difference between materials in this was obvious in the collected data, as presented later in this paper. With this in mind, it difficult to justify considering material choice as a factor and therefore, each material is considered to be a separate experiment with the same variables. In each case, the raster angle (due to the rectilinear print pattern; see Figure 2) and print orientation were considered as the variables, while all other parameters were fixed. The fixed parameters varied somewhat between materials due to the optimal printing parameters needed for each material. Only open-source raw material and processing equipment built and calibrated by the authors were used for this study in order to be able to take the maximum amount of control during processing. All print nozzles, relevant belts and bearings, and printer firmware were updated or replaced before making the samples to ensure that these things did not introduce unnecessary error into the specimens; the purpose of this was to isolate the observed error sources to material behavior and process mechanics.

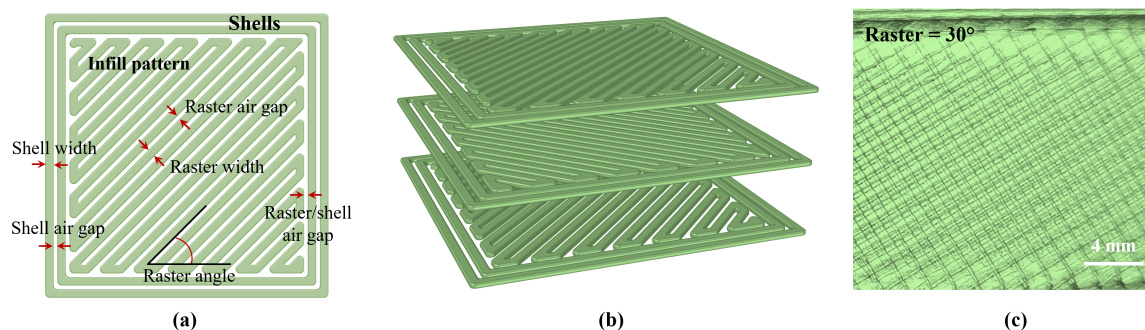


Figure 2. Rectilinear infill pattern for (a) a single layer, (b) multiple layers, and (c) observed in a manufactured sample at a raster angle of 30° and 100% density

Varying the raster angle changed the position of the part relative to the motion of the extruder carriage, so any overshoot or position error in the mechanics should produce variability in the precision of the parts relative to orientation. It is clear from Figure 2 that the rectilinear pattern would be influenced by this, which in turn would influence the accuracy of the whole part due to the cycling of the extruder while infilling the part. Material behavior also plays a role in this, as materials that collect residual stresses or shrink on cooling would cause the infill to retract slightly, potentially deforming the shell (see Figure 2a) and causing dimensional error in the part. Changing this orientation under these material conditions would change the force pattern inside the material from stresses, which can be reasonably expected to affect the dimensional accuracy of the parts. Since orientation of the part or part sections may not be a controllable variable during manufacturing, it is vital that the designer can understand and plan for such variability in some materials.

While varying the raster angle is an effective way to study the influence of the infill on the dimensional accuracy, the influence of the part shell needs to be studied by varying the print orientation. There are three basic potential sources of error from the shell, namely the build direction, the distance from the build plate, and the ratio of the shell to infill for each layer. In FDM, all the layers are deposited parallel to the build plate, with the shell being the first and most vital section of the part slice to be deposited, so the percentage of each layer that is shell should have a large influence on accuracy. Similarly, the distance from the build plate affects the heat distribution in the part, as a taller part will be warmer on the bottom during processing than the top. This heat differential can introduce residual stresses and cause cracks and warping in the shell.

Table 1. Materials, composition, and source

Material	Composition	Filament Source/Brand
1 ABS	Acrylonitrile butadiene styrene	Hatchbox ABS
2 PLA	Polylactic acid	Hatchbox PLA
3 HTPLA	High-temperature PLA	MakerGeeks Raptor PLA
4 HIPS	High-impact polystyrene	Monoprice premium natural
5 Nylon	Synthetic polyamide	eSUN ePA
6 PETG	Polyethylene terephthalate glycol-enhanced	Inland white
7 PC	Polycarbonate	eSUN black PC
8 APLA	PLA + 40% aluminum powder	SainSmart aluminum
9 CPLA	PLA + 5% copper powder	GizmoDorks copper
10 WPLA	PLA + 30%wood fiber	Hatchbox wood
11 CFPLA	PLA + 15% chopped carbon fibers	3DSolutech carbon fiber

Eleven materials were studied, as shown in Table 1. The sample design was that of the standard specimen for ASTM polymer impact testing [41]; this was chosen so that three different dimension scales of the same type of “feature” could be studied for each case to give a better understanding of the dimensional error observed. As a secondary consideration, this design was selected so that the samples could be re-used for other studies after testing and not wasted; they were not damaged during measurement, so they were suited for re-use. The specimen geometry is shown in Figure 3a below, where the nominal dimensions are:

$$Z = 3.25 \text{ mm}, \quad C = 63.5 \text{ mm}, \quad E = 12.7 \text{ mm}$$

The three print orientations selected were flat (Figure 3b), horizontal (Figure 3c), and vertical (Figure 3d). Two shells were used for each part, with a an infill percentage of each layer for the flat case estimated to be approximately 95%, while the infill percentages of the horizontal and vertical cases were found to be about 80% and 50%, respectively. Also for each material, a 90-degree sweep of raster angles in 15 degree increments was defined for the infill (Figure 3e). With the seven raster angles and three orientations, 21 unique combinations were produced. The decision was made to test each material case ten times to ensure a comprehensive dataset. This involved manufacturing and measuring 210 separate samples for each material, for a total of 2310 specimens and 6930 measurements. As with the parameter values, the measurement technique and assumptions are discussed in Section 3.

2.2. Calculation and Data Presentation

A summary of the results is presented in this report (Tables 2-12), but the entire dataset is attached as a supplement with this report and can be viewed and studied by the reader. For the set of samples

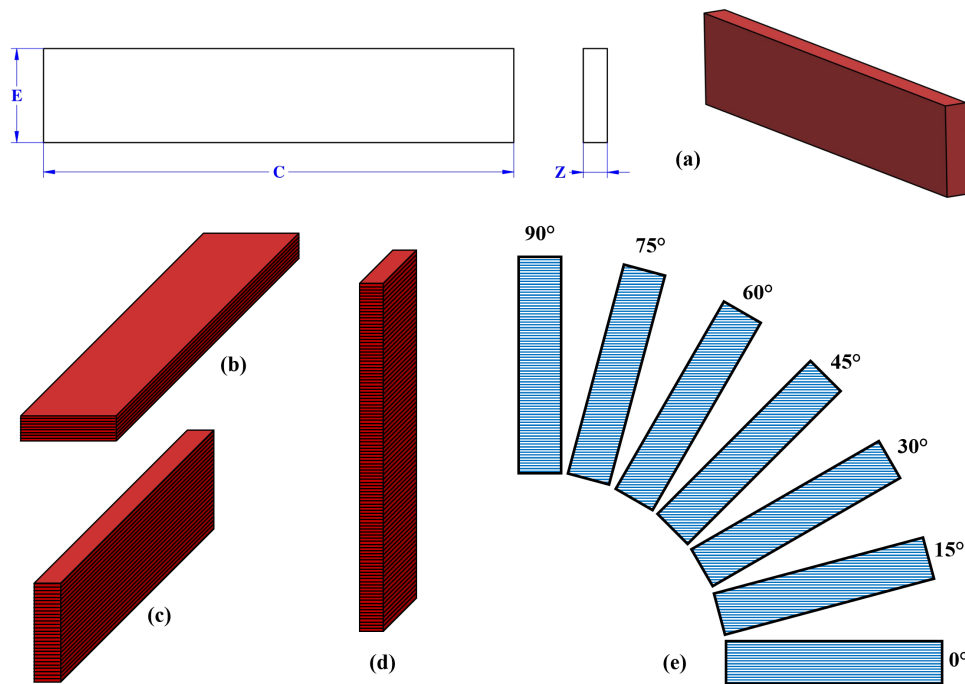


Figure 3. Specimen configurations: (a) standard geometry, (b) flat printing orientation, (c) horizontal printing orientation, (d) vertical printing orientation, and (e) raster angles

of each combination for each material, the three dimensions were measured and the dataset was summarized into four basic measures (Tables 2-12):

1. Sample mean μ : The average observed value of the dimension ($samplesize = 10$)
2. Nominal error $|\delta|$: The difference between the mean observed value and the nominal value
3. Standard error SE : Standard error based on the sample size and the standard deviation
4. Mean percent error MPE : Mean percent error of the dataset

Each of these measures assesses an important aspect about the dimensional accuracy of the samples. The full (raw) dataset is attached with this manuscript and can be viewed by the reader on demand. For each combination of print orientation and raster angle, the nominal error was defined as the absolute value of the difference between the mean and the nominal value such that

$$|\delta| = |X_{nom} - \mu| \quad (1)$$

where X_{nom} is the nominal value and μ is the mean of the n sample values. Next, the standard error was calculated as

$$SE = S / \sqrt{n} \quad (2)$$

where S is the standard deviation of the sample measurements and n is the number of measurements. Finally, the mean percent error was calculated as

$$MPE = \frac{100\%}{n} \sum_{t=1}^n \frac{a_t - f_t}{a_t} \quad (3)$$

where a_t is the observed value and f_t is the nominal dimension. After the set of measures were taken for each combination, a “combined” error measurement was taken for all three of the measured dimensions such that:

$$|\Delta| = \sqrt{|\delta_Z|^2 + |\delta_C|^2 + |\delta_E|^2} \quad (4)$$

The purpose of the nominal error ($|\delta|$) calculation was to find the deviation of the mean observed value from the nominal value; note that it is an absolute value and is only a measure of the *magnitude* of the error. The standard error (SE) measured the deviation from the sample mean and described the spread of the data, related to the observed values and not to the nominal values. Finally, the mean percent error (MPE) was a measure of the average deviation from the nominal value on the level of each sample in the set; note that it is directional, noting both positive and negative errors.

Each of the materials under study are presented in the preceding sections, each consisting of three parts: a color image showing the 21 samples for one replication of the experiment, a set of plots showing $|\delta|$ and MPE for each of the dimensional measurements, and a table summarizing the statistical measures described above.

2.3. Acrylonitrile Butadiene Styrene (ABS)

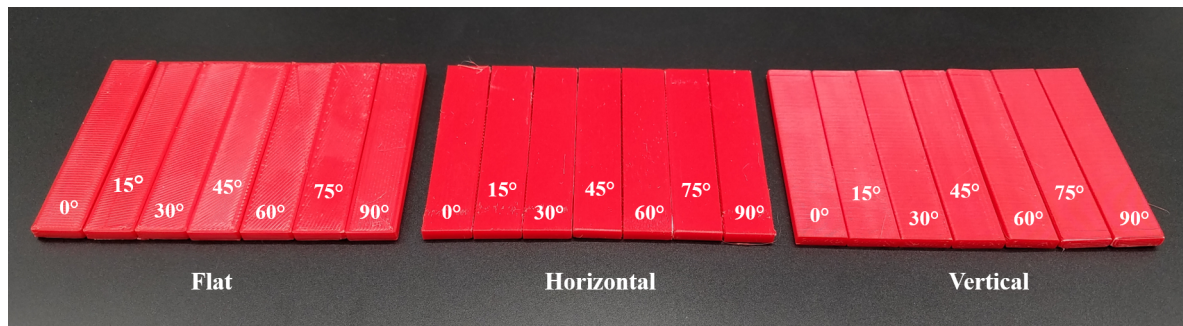


Figure 4. ABS specimen set for one replication of measurements

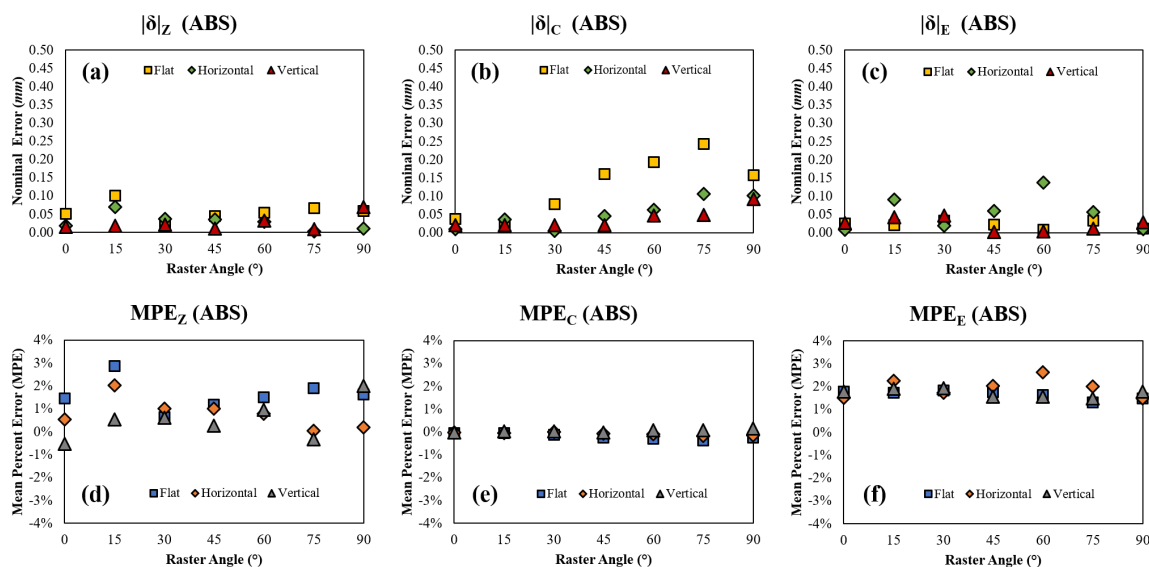


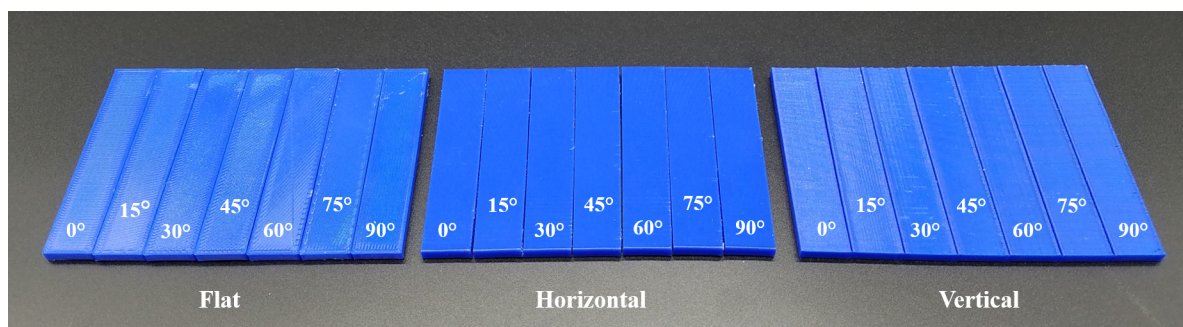
Figure 5. ABS (a) nominal error in Z, (b) nominal error in C, (c) nominal error in E, (d) mean percent error in Z, (e) mean percent error in C, and (f) mean percent error in E with respect to raster angle and orientation

Table 2. Mean, $|\delta|$, SE, MPE, and $|\Delta|$ for ABS as a function of print orientation and raster angle

Material: ABS (all dimensions in mm unless otherwise specified)

PO	Angle	Z ($n = 10$)				C ($n = 10$)				E ($n = 10$)				$ \Delta $
		μ	$ \delta $	SE	MPE	μ	$ \delta $	SE	MPE	μ	$ \delta $	SE	MPE	
F	0°	3.30	0.05	0.034	1.45%	63.46	0.04	0.024	-0.06%	12.73	0.03	0.014	1.77%	0.07
F	15°	3.35	0.10	0.040	2.86%	63.48	0.02	0.065	-0.03%	12.72	0.02	0.015	1.74%	0.10
F	30°	3.28	0.03	0.043	0.64%	63.42	0.08	0.029	-0.12%	12.73	0.03	0.018	1.83%	0.09
F	45°	3.29	0.04	0.042	1.19%	63.34	0.16	0.033	-0.25%	12.72	0.02	0.013	1.75%	0.17
F	60°	3.30	0.05	0.040	1.50%	63.31	0.19	0.033	-0.31%	12.71	0.01	0.023	1.63%	0.20
F	75°	3.32	0.07	0.040	1.89%	63.26	0.24	0.047	-0.38%	12.67	0.03	0.026	1.31%	0.25
F	90°	3.31	0.06	0.043	1.64%	63.34	0.16	0.038	-0.25%	12.69	0.01	0.013	1.48%	0.17
H	0°	3.27	0.02	0.015	0.53%	63.49	0.01	0.015	-0.02%	12.69	0.01	0.018	1.50%	0.02
H	15°	3.32	0.07	0.027	2.02%	63.46	0.04	0.014	-0.06%	12.79	0.09	0.024	2.26%	0.12
H	30°	3.29	0.04	0.036	1.02%	63.50	0.00	0.014	-0.01%	12.72	0.02	0.015	1.73%	0.04
H	45°	3.29	0.04	0.031	1.01%	63.45	0.05	0.015	-0.07%	12.76	0.06	0.021	2.04%	0.08
H	60°	3.28	0.03	0.033	0.79%	63.44	0.06	0.012	-0.10%	12.84	0.14	0.026	2.63%	0.15
H	75°	3.25	0.00	0.024	0.04%	63.39	0.11	0.015	-0.17%	12.76	0.06	0.015	2.01%	0.12
H	90°	3.26	0.01	0.038	0.19%	63.40	0.10	0.030	-0.16%	12.69	0.01	0.033	1.49%	0.10
V	0°	3.24	0.01	0.026	-0.52%	63.48	0.02	0.042	-0.03%	12.73	0.03	0.013	1.78%	0.04
V	15°	3.27	0.02	0.023	0.54%	63.52	0.02	0.028	0.03%	12.74	0.04	0.015	1.91%	0.05
V	30°	3.27	0.02	0.016	0.62%	63.52	0.02	0.037	0.03%	12.75	0.05	0.011	1.94%	0.06
V	45°	3.26	0.01	0.019	0.28%	63.48	0.02	0.029	-0.03%	12.70	0.00	0.018	1.56%	0.02
V	60°	3.28	0.03	0.022	0.96%	63.55	0.05	0.049	0.07%	12.70	0.00	0.014	1.55%	0.06
V	75°	3.24	0.01	0.023	-0.32%	63.55	0.05	0.054	0.08%	12.69	0.01	0.018	1.49%	0.05
V	90°	3.32	0.07	0.030	2.01%	63.59	0.09	0.044	0.15%	12.73	0.03	0.009	1.79%	0.12

2.4. Polylactic Acid (PLA)

**Figure 6.** PLA specimen set for one replication of measurements

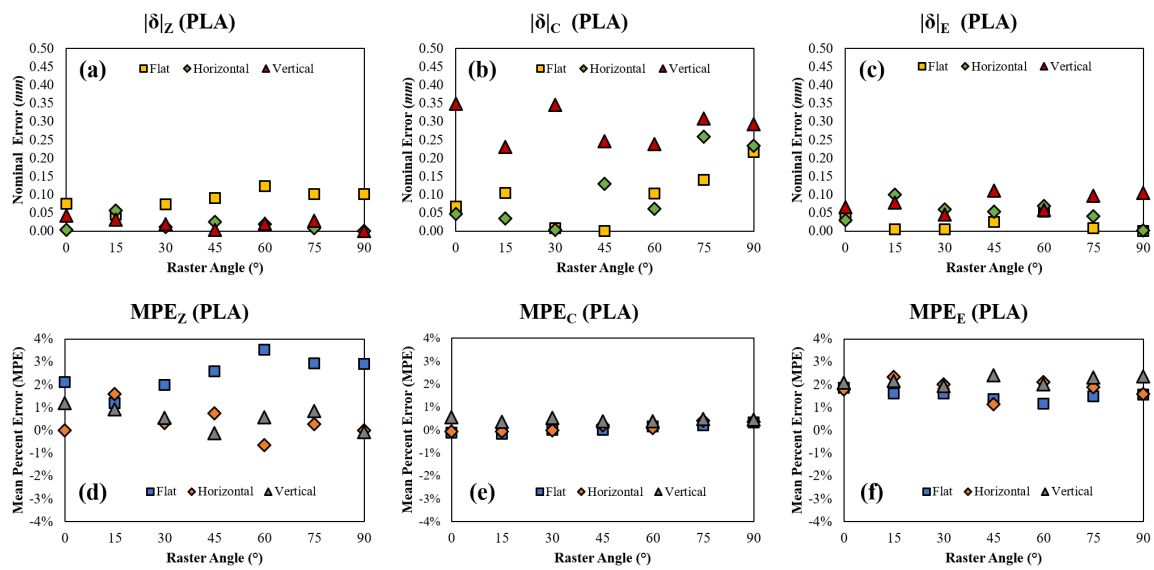


Figure 7. PLA (a) nominal error in Z, (b) nominal error in C, (c) nominal error in E, (d) mean percent error in Z, (e) mean percent error in C, and (f) mean percent error in E with respect to raster angle and orientation

Table 3. Mean, $|\delta|$, SE, MPE, and $|\Delta|$ for PLA as a function of print orientation and raster angle

Material: PLA (all dimensions in mm unless otherwise specified)														
PO	Angle	Z ($n = 10$)				C ($n = 10$)				E ($n = 10$)				$ \Delta $
		μ	$ \delta $	SE	MPE	μ	$ \delta $	SE	MPE	μ	$ \delta $	SE	MPE	
F	0°	3.33	0.08	0.044	2.10%	63.43	0.07	0.014	-0.11%	12.74	0.04	0.019	1.87%	0.11
F	15°	3.30	0.05	0.045	1.20%	63.40	0.10	0.017	-0.17%	12.71	0.01	0.028	1.62%	0.11
F	30°	3.32	0.07	0.052	1.98%	63.51	0.01	0.012	0.01%	12.71	0.01	0.016	1.62%	0.07
F	45°	3.34	0.09	0.043	2.58%	63.50	0.00	0.011	0.00%	12.67	0.03	0.019	1.37%	0.09
F	60°	3.37	0.12	0.043	3.54%	63.60	0.10	0.031	0.16%	12.65	0.05	0.026	1.16%	0.17
F	75°	3.35	0.10	0.033	2.93%	63.64	0.14	0.020	0.22%	12.69	0.01	0.027	1.50%	0.17
F	90°	3.35	0.10	0.041	2.91%	63.72	0.22	0.021	0.34%	12.70	0.00	0.017	1.57%	0.24
H	0°	3.25	0.00	0.032	0.01%	63.45	0.05	0.020	-0.07%	12.73	0.03	0.031	1.80%	0.06
H	15°	3.31	0.06	0.039	1.60%	63.47	0.04	0.022	-0.06%	12.80	0.10	0.054	2.33%	0.12
H	30°	3.26	0.01	0.025	0.31%	63.50	0.00	0.012	-0.01%	12.76	0.06	0.039	2.02%	0.06
H	45°	3.28	0.03	0.025	0.74%	63.63	0.13	0.027	0.20%	12.65	0.05	0.063	1.13%	0.14
H	60°	3.23	0.02	0.020	-0.65%	63.56	0.06	0.028	0.10%	12.77	0.07	0.019	2.10%	0.09
H	75°	3.26	0.01	0.010	0.27%	63.76	0.26	0.055	0.40%	12.74	0.04	0.023	1.89%	0.26
H	90°	3.25	0.00	0.018	0.00%	63.73	0.23	0.059	0.37%	12.70	0.00	0.025	1.59%	0.23
V	0°	3.29	0.04	0.032	1.20%	63.85	0.35	0.024	0.55%	12.77	0.07	0.028	2.08%	0.36
V	15°	3.28	0.03	0.023	0.93%	63.73	0.23	0.050	0.36%	12.78	0.08	0.039	2.17%	0.25
V	30°	3.27	0.02	0.020	0.55%	63.85	0.35	0.024	0.54%	12.75	0.05	0.019	1.93%	0.35
V	45°	3.25	0.00	0.021	-0.13%	63.75	0.25	0.053	0.39%	12.81	0.11	0.032	2.42%	0.27
V	60°	3.27	0.02	0.027	0.58%	63.74	0.24	0.051	0.37%	12.76	0.06	0.030	2.02%	0.25
V	75°	3.28	0.03	0.020	0.85%	63.81	0.31	0.025	0.48%	12.80	0.10	0.032	2.32%	0.33
V	90°	3.25	0.00	0.021	-0.07%	63.79	0.29	0.017	0.46%	12.80	0.10	0.032	2.37%	0.31

2.5. High-Temperature PLA (HTPLA)

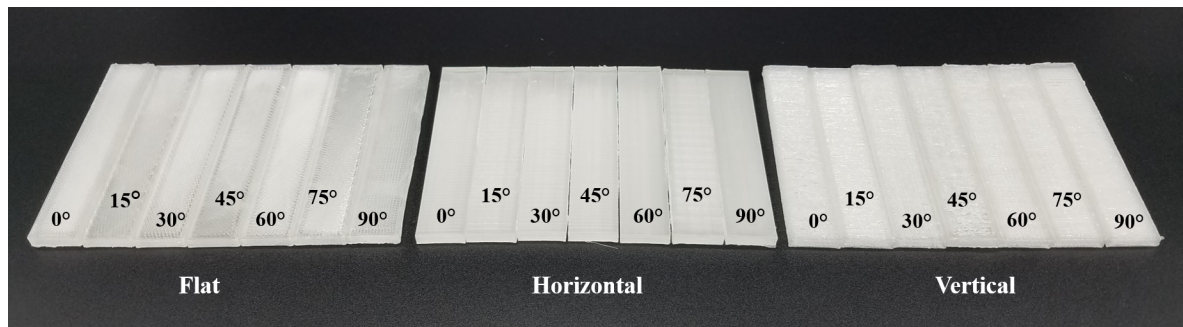


Figure 8. HTPLA specimen set for one replication of measurements

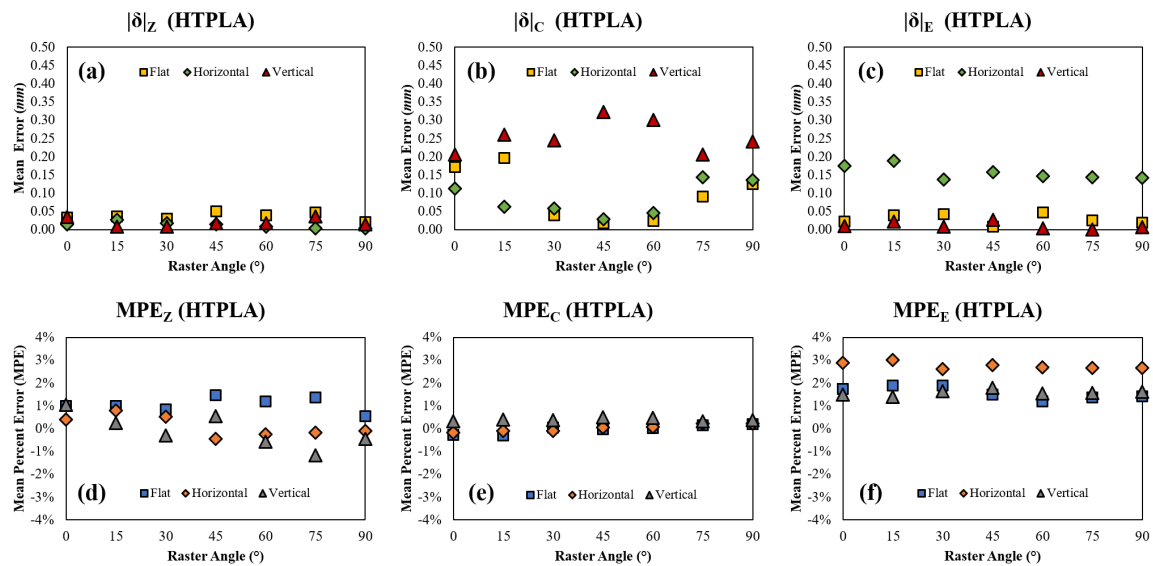


Figure 9. HTPLA (a) nominal error in Z, (b) nominal error in C, (c) nominal error in E, (d) mean percent error in Z, (e) mean percent error in C, and (f) mean percent error in E with respect to raster angle and orientation

Table 4. Mean, $|\delta|$, SE, MPE, and $|\Delta|$ for HTPLA as a function of print orientation and raster angle

Material: HTPLA (all dimensions in mm unless otherwise specified)														
PO	Angle	Z ($n = 10$)				C ($n = 10$)				E ($n = 10$)				$ \Delta $
		μ	$ \delta $	SE	MPE	μ	$ \delta $	SE	MPE	μ	$ \delta $	SE	MPE	
F	0°	3.28	0.03	0.022	1.00%	63.33	0.17	0.026	-0.27%	12.72	0.02	0.023	1.75%	0.18
F	15°	3.29	0.04	0.033	1.00%	63.30	0.20	0.014	-0.31%	12.74	0.04	0.030	1.88%	0.20
F	30°	3.28	0.03	0.029	0.84%	63.54	0.04	0.043	0.06%	12.74	0.04	0.023	1.90%	0.06
F	45°	3.30	0.05	0.023	1.47%	63.48	0.02	0.020	-0.03%	12.69	0.01	0.030	1.50%	0.05
F	60°	3.29	0.04	0.019	1.19%	63.52	0.02	0.028	0.04%	12.65	0.05	0.014	1.20%	0.07
F	75°	3.30	0.05	0.029	1.36%	63.59	0.09	0.033	0.14%	12.68	0.03	0.036	1.37%	0.11
F	90°	3.27	0.02	0.033	0.55%	63.63	0.13	0.019	0.20%	12.68	0.02	0.013	1.43%	0.13
H	0°	3.26	0.01	0.021	0.39%	63.39	0.11	0.027	-0.18%	12.87	0.17	0.041	2.90%	0.21

H	15°	3.28	0.03	0.018	0.80%	63.44	0.06	0.024	-0.10%	12.89	0.19	0.027	3.01%	0.20
H	30°	3.27	0.02	0.007	0.52%	63.44	0.06	0.019	-0.09%	12.84	0.14	0.040	2.62%	0.15
H	45°	3.24	0.01	0.010	-0.44%	63.53	0.03	0.011	0.04%	12.86	0.16	0.036	2.78%	0.16
H	60°	3.24	0.01	0.012	-0.26%	63.55	0.05	0.022	0.07%	12.85	0.15	0.025	2.69%	0.15
H	75°	3.25	0.00	0.024	-0.17%	63.64	0.14	0.022	0.22%	12.84	0.14	0.023	2.67%	0.20
H	90°	3.25	0.00	0.013	-0.11%	63.64	0.14	0.033	0.21%	12.84	0.14	0.037	2.66%	0.20
V	0°	3.29	0.04	0.019	1.03%	63.71	0.20	0.077	0.32%	12.69	0.01	0.019	1.50%	0.21
V	15°	3.26	0.01	0.009	0.24%	63.76	0.26	0.036	0.41%	12.68	0.02	0.011	1.40%	0.26
V	30°	3.24	0.01	0.010	-0.29%	63.74	0.24	0.082	0.38%	12.71	0.01	0.006	1.64%	0.24
V	45°	3.27	0.02	0.012	0.54%	63.82	0.32	0.038	0.51%	12.73	0.03	0.016	1.78%	0.32
V	60°	3.23	0.02	0.012	-0.57%	63.80	0.30	0.061	0.47%	12.70	0.00	0.018	1.55%	0.30
V	75°	3.21	0.04	0.014	-1.17%	63.71	0.21	0.075	0.32%	12.70	0.00	0.013	1.57%	0.21
V	90°	3.24	0.01	0.006	-0.44%	63.74	0.24	0.047	0.38%	12.71	0.01	0.006	1.63%	0.24

2.6. High-Impact Polystyrene (HIPS)

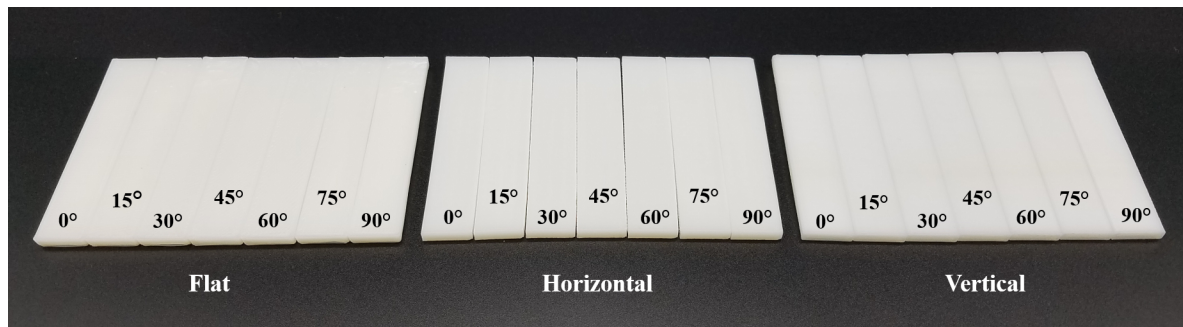


Figure 10. HIPS (a) nominal error in Z, (b) nominal error in C, (c) nominal error in E, (d) mean percent error in Z, (e) mean percent error in C, and (f) mean percent error in E with respect to raster angle and orientation

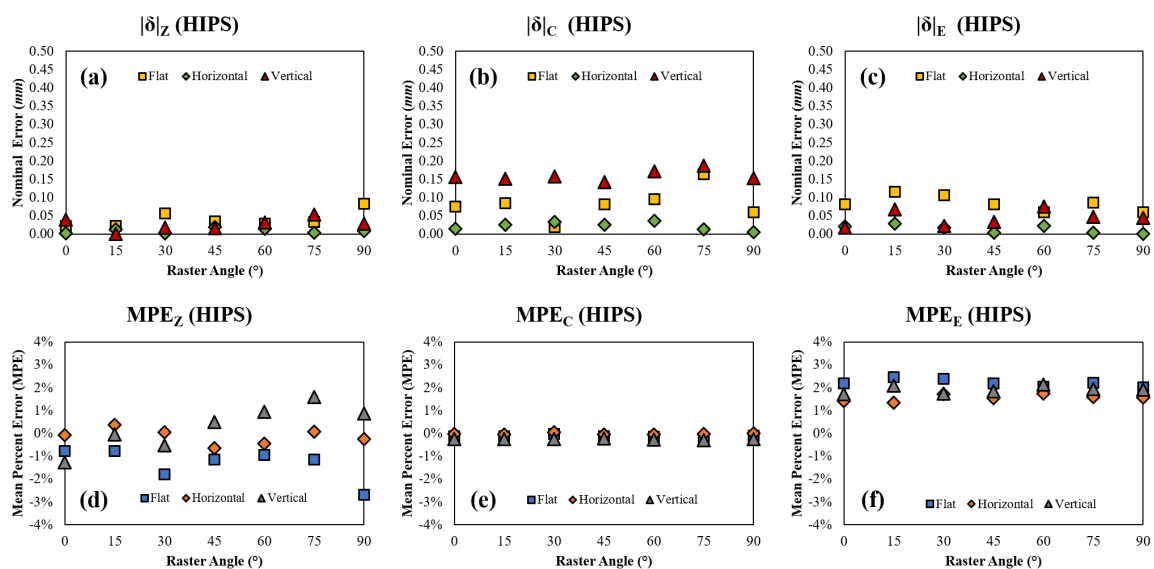


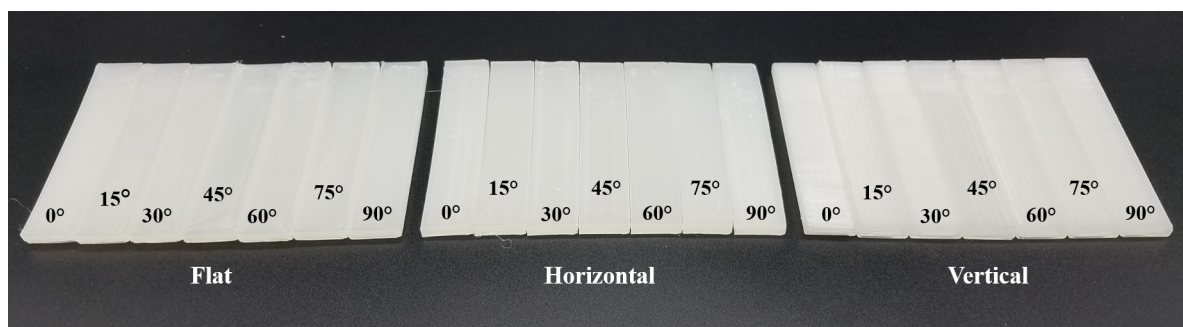
Figure 11. Nominal error for HTPLA with respect to raster angle and orientation

Table 5. Mean, $|\delta|$, SE, MPE, and $|\Delta|$ for HIPS as a function of print orientation and raster angle

Material: HIPS (all dimensions in *mm* unless otherwise specified)

PO	Angle	Z (<i>n</i> = 10)				C (<i>n</i> = 10)				E (<i>n</i> = 10)				$ \Delta $
		μ	$ \delta $	SE	MPE	μ	$ \delta $	SE	MPE	μ	$ \delta $	SE	MPE	
F	0°	3.23	0.02	0.034	-0.78%	63.42	0.08	0.030	-0.12%	12.78	0.08	0.050	2.19%	0.11
F	15°	3.23	0.02	0.026	-0.77%	63.42	0.09	0.027	-0.13%	12.82	0.12	0.048	2.45%	0.15
F	30°	3.19	0.06	0.020	-1.79%	63.48	0.02	0.035	-0.03%	12.81	0.11	0.041	2.38%	0.12
F	45°	3.22	0.04	0.022	-1.13%	63.42	0.08	0.030	-0.13%	12.78	0.08	0.041	2.19%	0.12
F	60°	3.22	0.03	0.028	-0.94%	63.40	0.10	0.031	-0.15%	12.76	0.06	0.040	2.03%	0.12
F	75°	3.22	0.03	0.035	-1.13%	63.34	0.16	0.032	-0.26%	12.79	0.09	0.049	2.22%	0.19
F	90°	3.17	0.08	0.026	-2.68%	63.44	0.06	0.027	-0.09%	12.76	0.06	0.055	2.01%	0.12
H	0°	3.25	0.00	0.011	-0.07%	63.49	0.02	0.023	-0.02%	12.68	0.02	0.028	1.41%	0.03
H	15°	3.26	0.01	0.016	0.38%	63.48	0.02	0.020	-0.04%	12.67	0.03	0.016	1.35%	0.04
H	30°	3.25	0.00	0.008	0.06%	63.53	0.03	0.015	0.05%	12.72	0.02	0.020	1.70%	0.04
H	45°	3.23	0.02	0.013	-0.63%	63.48	0.02	0.016	-0.04%	12.70	0.00	0.028	1.54%	0.03
H	60°	3.24	0.01	0.007	-0.44%	63.46	0.04	0.016	-0.06%	12.72	0.02	0.026	1.75%	0.05
H	75°	3.25	0.00	0.010	0.08%	63.49	0.01	0.024	-0.02%	12.70	0.00	0.024	1.60%	0.01
H	90°	3.24	0.01	0.009	-0.25%	63.51	0.01	0.012	0.01%	12.70	0.00	0.018	1.57%	0.01
V	0°	3.21	0.04	0.011	-1.26%	63.34	0.16	0.043	-0.25%	12.72	0.02	0.016	1.70%	0.16
V	15°	3.25	0.00	0.008	-0.04%	63.35	0.15	0.045	-0.24%	12.77	0.07	0.023	2.09%	0.17
V	30°	3.23	0.02	0.009	-0.53%	63.34	0.16	0.039	-0.25%	12.72	0.02	0.017	1.75%	0.16
V	45°	3.27	0.02	0.006	0.49%	63.36	0.14	0.036	-0.22%	12.73	0.03	0.012	1.83%	0.15
V	60°	3.28	0.03	0.009	0.94%	63.33	0.17	0.030	-0.27%	12.78	0.08	0.020	2.15%	0.19
V	75°	3.30	0.05	0.015	1.59%	63.31	0.19	0.028	-0.30%	12.75	0.05	0.024	1.94%	0.20
V	90°	3.28	0.03	0.014	0.87%	63.35	0.15	0.045	-0.24%	12.74	0.04	0.014	1.91%	0.16

2.7. Synthetic Polyamide (Nylon)

**Figure 12.** Nylon specimen set for one replication of measurements

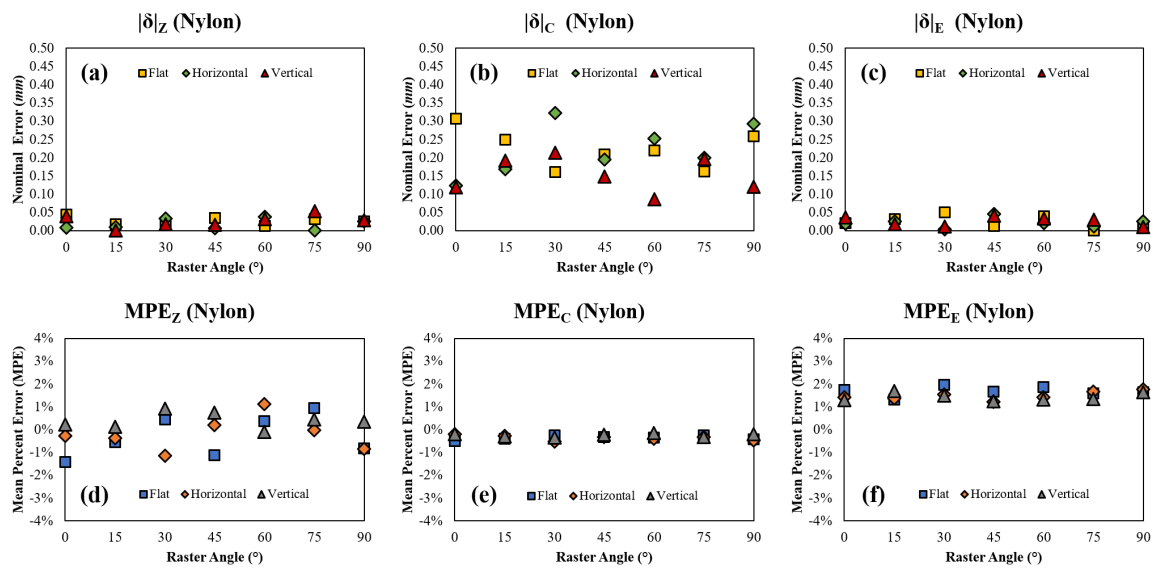


Figure 13. Nylon (a) nominal error in Z, (b) nominal error in C, (c) nominal error in E, (d) mean percent error in Z, (e) mean percent error in C, and (f) mean percent error in E with respect to raster angle and orientation

Table 6. Mean, $|\delta|$, SE, MPE, and $|\Delta|$ for nylon as a function of print orientation and raster angle

Material: Nylon (all dimensions in mm unless otherwise specified)														
PO	Angle	Z ($n = 10$)				C ($n = 10$)				E ($n = 10$)				$ \Delta $
		μ	$ \delta $	SE	MPE	μ	$ \delta $	SE	MPE	μ	$ \delta $	SE	MPE	
F	0°	3.21	0.04	0.020	-1.41%	63.19	0.31	0.105	-0.49%	12.72	0.02	0.028	1.73%	0.31
F	15°	3.23	0.02	0.018	-0.55%	63.25	0.25	0.100	-0.40%	12.67	0.03	0.031	1.33%	0.25
F	30°	3.27	0.01	0.016	0.44%	63.34	0.16	0.086	-0.25%	12.75	0.05	0.028	1.96%	0.17
F	45°	3.22	0.04	0.016	-1.11%	63.29	0.21	0.102	-0.33%	12.71	0.01	0.024	1.67%	0.21
F	60°	3.26	0.01	0.014	0.38%	63.28	0.22	0.121	-0.35%	12.74	0.04	0.032	1.87%	0.22
F	75°	3.28	0.03	0.016	0.95%	63.34	0.16	0.114	-0.26%	12.70	0.00	0.016	1.58%	0.17
F	90°	3.22	0.03	0.015	-0.83%	63.24	0.26	0.103	-0.41%	12.71	0.01	0.038	1.64%	0.26
H	0°	3.24	0.01	0.021	-0.28%	63.38	0.12	0.110	-0.20%	12.68	0.02	0.018	1.43%	0.13
H	15°	3.24	0.01	0.025	-0.36%	63.33	0.17	0.093	-0.27%	12.67	0.03	0.022	1.37%	0.17
H	30°	3.22	0.03	0.031	-1.14%	63.18	0.32	0.095	-0.51%	12.70	0.00	0.009	1.55%	0.32
H	45°	3.26	0.01	0.017	0.19%	63.31	0.20	0.100	-0.31%	12.66	0.05	0.021	1.22%	0.20
H	60°	3.29	0.04	0.022	1.12%	63.25	0.25	0.111	-0.40%	12.68	0.02	0.018	1.41%	0.26
H	75°	3.25	0.00	0.018	-0.03%	63.30	0.20	0.093	-0.32%	12.71	0.01	0.016	1.66%	0.20
H	90°	3.22	0.03	0.024	-0.86%	63.21	0.29	0.092	-0.47%	12.73	0.03	0.013	1.77%	0.30
V	0°	3.26	0.01	0.019	0.21%	63.38	0.12	0.061	-0.19%	12.66	0.04	0.012	1.29%	0.12
V	15°	3.25	0.00	0.010	0.12%	63.31	0.19	0.045	-0.30%	12.72	0.02	0.034	1.70%	0.19
V	30°	3.28	0.03	0.013	0.93%	63.29	0.21	0.063	-0.34%	12.69	0.01	0.028	1.49%	0.22
V	45°	3.28	0.02	0.014	0.75%	63.35	0.15	0.073	-0.23%	12.66	0.04	0.013	1.26%	0.16
V	60°	3.25	0.00	0.009	-0.10%	63.41	0.09	0.054	-0.14%	12.67	0.03	0.025	1.31%	0.09
V	75°	3.27	0.01	0.005	0.46%	63.30	0.20	0.055	-0.31%	12.67	0.03	0.014	1.34%	0.20
V	90°	3.26	0.01	0.013	0.35%	63.38	0.12	0.062	-0.19%	12.71	0.01	0.014	1.65%	0.12

2.8. Polyethylene Terephthalate Glycol-Enhanced (PETG)

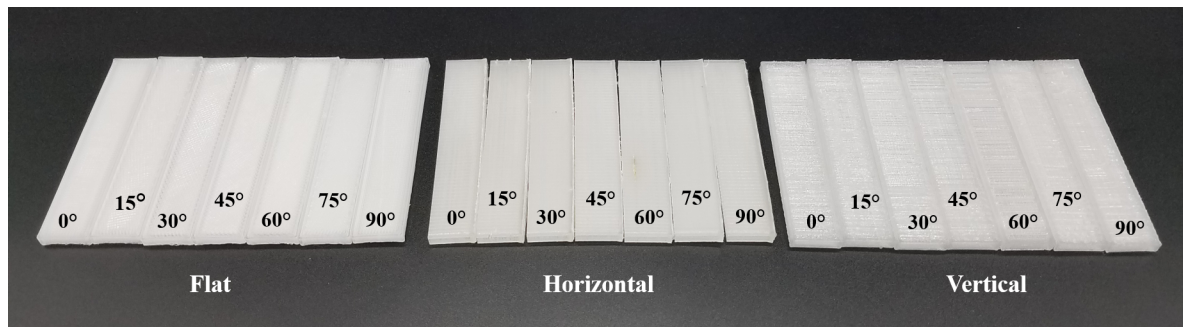


Figure 14. PETG specimen set for one replication of measurements

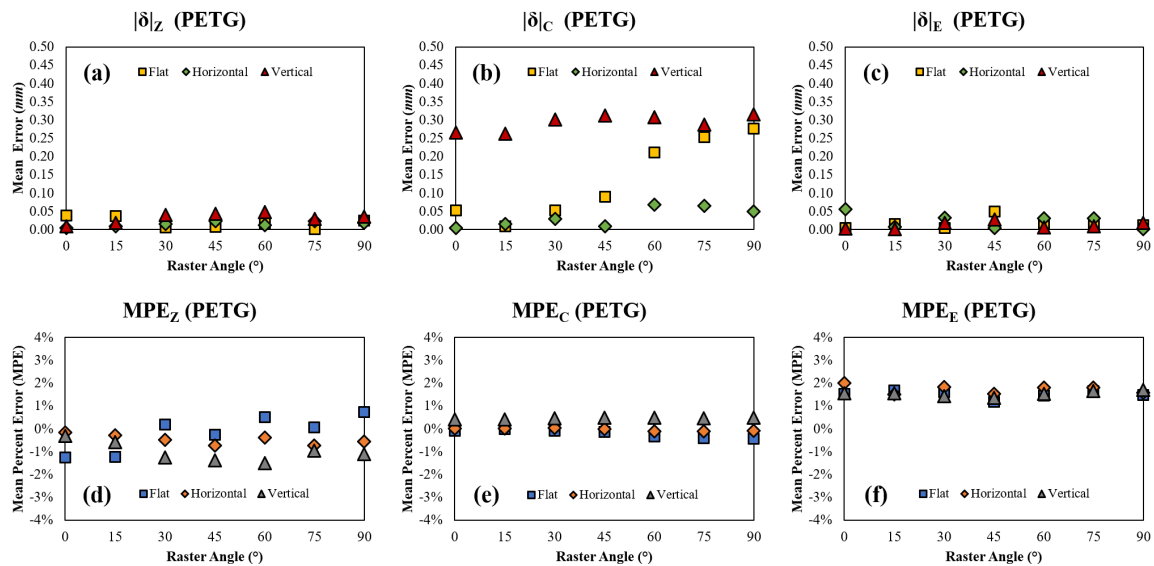


Figure 15. PETG (a) nominal error in Z, (b) nominal error in C, (c) nominal error in E, (d) mean percent error in Z, (e) mean percent error in C, and (f) mean percent error in E with respect to raster angle and orientation

Table 7. Mean, $|\delta|$, SE, MPE, and $|\Delta|$ for PETG as a function of print orientation and raster angle

Material: PETG (all dimensions in mm unless otherwise specified)														
PO	Angle	Z ($n = 10$)				C ($n = 10$)				E ($n = 10$)				$ \Delta $
		μ	$ \delta $	SE	MPE	μ	$ \delta $	SE	MPE	μ	$ \delta $	SE	MPE	
F	0°	3.21	0.04	0.023	-1.26%	63.45	0.05	0.042	-0.08%	12.70	0.00	0.015	1.54%	0.07
F	15°	3.21	0.04	0.020	-1.22%	63.49	0.01	0.013	-0.01%	12.72	0.02	0.015	1.69%	0.04
F	30°	3.26	0.01	0.006	0.18%	63.45	0.05	0.044	-0.08%	12.71	0.01	0.018	1.61%	0.05
F	45°	3.24	0.01	0.014	-0.26%	63.41	0.09	0.034	-0.14%	12.65	0.05	0.019	1.19%	0.10
F	60°	3.27	0.02	0.010	0.51%	63.29	0.21	0.036	-0.34%	12.68	0.02	0.013	1.45%	0.21
F	75°	3.25	0.00	0.009	0.05%	63.25	0.25	0.046	-0.40%	12.71	0.01	0.026	1.66%	0.25
F	90°	3.28	0.02	0.017	0.74%	63.22	0.28	0.069	-0.44%	12.69	0.01	0.012	1.48%	0.28
H	0°	3.25	0.00	0.010	-0.16%	63.50	0.00	0.026	0.01%	12.76	0.06	0.011	2.01%	0.06

H	15°	3.24	0.01	0.013	-0.29%	63.52	0.02	0.024	0.03%	12.69	0.01	0.018	1.51%	0.02
H	30°	3.24	0.01	0.013	-0.48%	63.53	0.03	0.029	0.05%	12.73	0.03	0.020	1.83%	0.05
H	45°	3.23	0.02	0.009	-0.72%	63.49	0.01	0.015	-0.01%	12.70	0.00	0.029	1.54%	0.03
H	60°	3.24	0.01	0.010	-0.38%	63.43	0.07	0.034	-0.11%	12.73	0.03	0.015	1.81%	0.08
H	75°	3.23	0.02	0.011	-0.72%	63.44	0.06	0.056	-0.10%	12.73	0.03	0.028	1.81%	0.08
H	90°	3.23	0.02	0.008	-0.56%	63.45	0.05	0.053	-0.08%	12.70	0.00	0.010	1.58%	0.05
V	0°	3.24	0.01	0.010	-0.32%	63.77	0.27	0.031	0.42%	12.70	0.00	0.019	1.55%	0.27
V	15°	3.23	0.02	0.006	-0.59%	63.76	0.26	0.040	0.41%	12.70	0.00	0.019	1.57%	0.26
V	30°	3.21	0.04	0.013	-1.26%	63.80	0.30	0.042	0.47%	12.68	0.02	0.021	1.43%	0.31
V	45°	3.21	0.04	0.011	-1.38%	63.81	0.31	0.045	0.49%	12.67	0.03	0.015	1.36%	0.32
V	60°	3.20	0.05	0.007	-1.50%	63.81	0.31	0.051	0.48%	12.69	0.01	0.014	1.53%	0.31
V	75°	3.22	0.03	0.015	-0.95%	63.79	0.29	0.027	0.45%	12.71	0.01	0.010	1.64%	0.29
V	90°	3.22	0.04	0.017	-1.11%	63.82	0.31	0.019	0.49%	12.72	0.02	0.024	1.71%	0.32

2.9. Polycarbonate (PC)

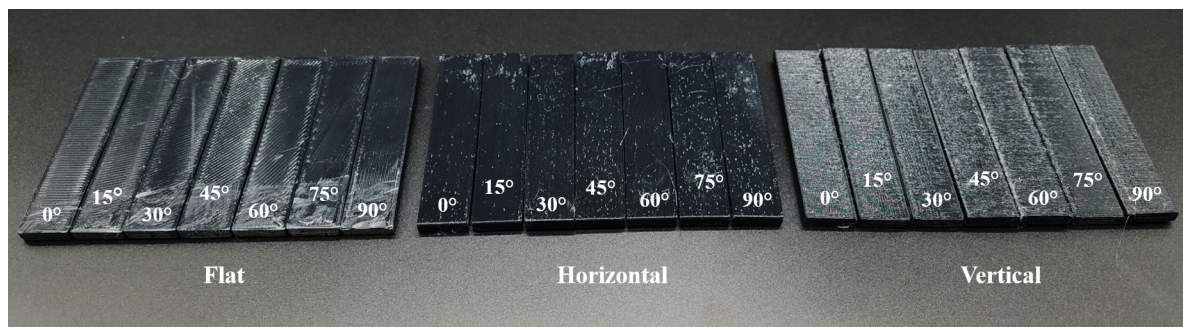


Figure 16. PC specimen set for one replication of measurements

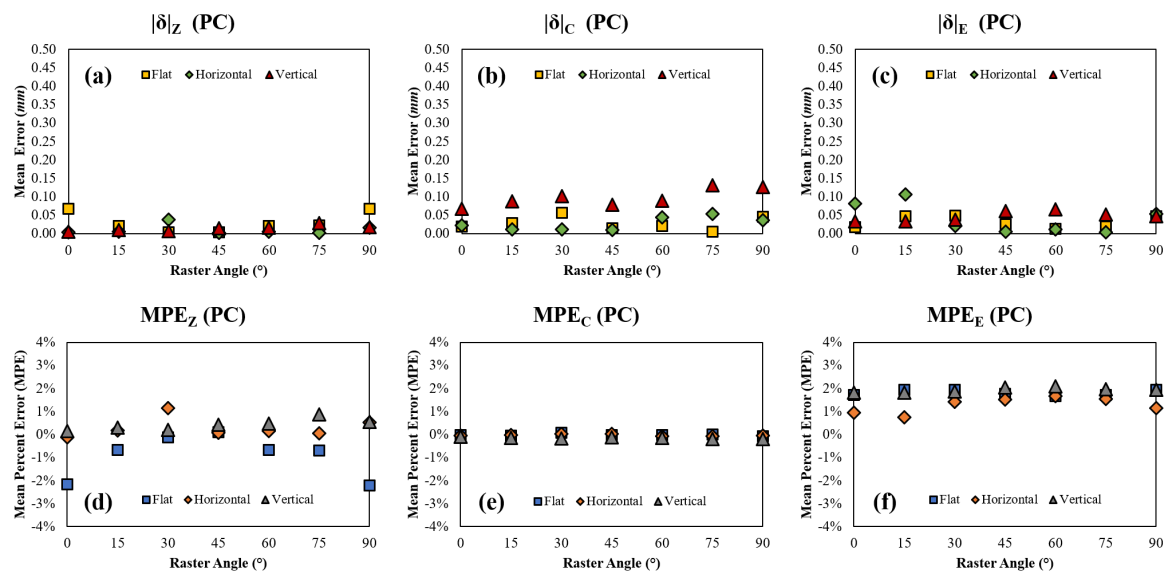


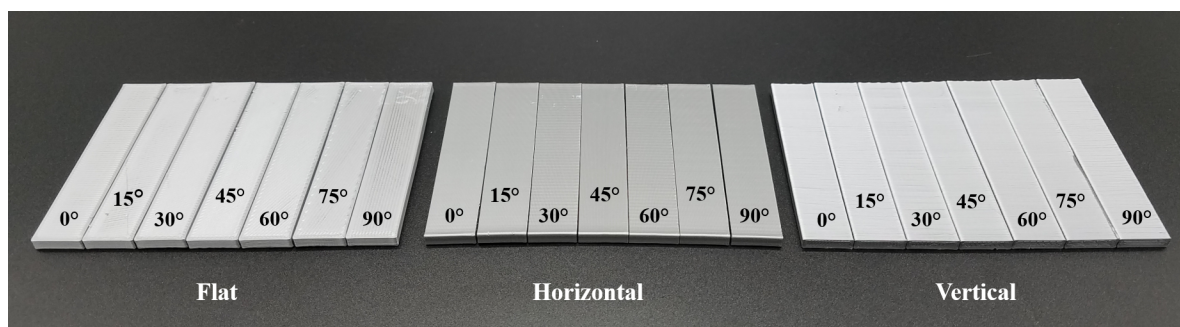
Figure 17. PC (a) nominal error in Z, (b) nominal error in C, (c) nominal error in E, (d) mean percent error in Z, (e) mean percent error in C, and (f) mean percent error in E with respect to raster angle and orientation

Table 8. Mean, $|\delta|$, SE, MPE, and $|\Delta|$ for PC as a function of print orientation and raster angle

Material: PC (all dimensions in mm unless otherwise specified)

PO	Angle	Z ($n = 10$)				C ($n = 10$)				E ($n = 10$)				$ \Delta $
		μ	$ \delta $	SE	MPE	μ	$ \delta $	SE	MPE	μ	$ \delta $	SE	MPE	
F	0°	3.18	0.07	0.017	-2.16%	63.48	0.02	0.031	-0.03%	12.72	0.02	0.016	1.71%	0.07
F	15°	3.23	0.02	0.009	-0.66%	63.47	0.03	0.023	-0.04%	12.75	0.05	0.017	1.94%	0.06
F	30°	3.25	0.00	0.010	-0.13%	63.56	0.06	0.034	0.09%	12.75	0.05	0.021	1.95%	0.08
F	45°	3.25	0.00	0.010	0.11%	63.49	0.01	0.030	-0.02%	12.73	0.03	0.013	1.77%	0.03
F	60°	3.23	0.02	0.012	-0.66%	63.48	0.02	0.034	-0.03%	12.71	0.01	0.010	1.67%	0.03
F	75°	3.23	0.02	0.014	-0.70%	63.49	0.01	0.014	-0.01%	12.72	0.02	0.019	1.73%	0.03
F	90°	3.18	0.07	0.029	-2.22%	63.45	0.05	0.027	-0.07%	12.75	0.05	0.016	1.94%	0.10
H	0°	3.25	0.00	0.004	-0.12%	63.48	0.02	0.015	-0.04%	12.62	0.08	0.031	0.94%	0.08
H	15°	3.26	0.01	0.009	0.18%	63.49	0.01	0.014	-0.02%	12.59	0.11	0.030	0.74%	0.11
H	30°	3.29	0.04	0.014	1.14%	63.51	0.01	0.013	0.02%	12.68	0.02	0.022	1.41%	0.05
H	45°	3.25	0.00	0.007	0.09%	63.51	0.01	0.015	0.02%	12.69	0.01	0.018	1.53%	0.01
H	60°	3.26	0.01	0.009	0.15%	63.46	0.04	0.029	-0.07%	12.71	0.01	0.014	1.67%	0.05
H	75°	3.25	0.00	0.008	0.06%	63.45	0.05	0.024	-0.08%	12.70	0.00	0.016	1.54%	0.05
H	90°	3.27	0.02	0.008	0.51%	63.46	0.04	0.024	-0.06%	12.65	0.05	0.029	1.15%	0.07
V	0°	3.26	0.01	0.010	0.15%	63.43	0.07	0.029	-0.11%	12.73	0.03	0.006	1.83%	0.08
V	15°	3.26	0.01	0.006	0.30%	63.41	0.09	0.022	-0.14%	12.73	0.03	0.008	1.83%	0.09
V	30°	3.26	0.01	0.004	0.21%	63.40	0.10	0.014	-0.16%	12.74	0.04	0.012	1.87%	0.11
V	45°	3.26	0.01	0.011	0.42%	63.42	0.08	0.027	-0.12%	12.76	0.06	0.015	2.04%	0.10
V	60°	3.27	0.02	0.008	0.49%	63.41	0.09	0.017	-0.14%	12.77	0.07	0.013	2.08%	0.11
V	75°	3.28	0.03	0.012	0.87%	63.37	0.13	0.032	-0.21%	12.75	0.05	0.013	1.98%	0.14
V	90°	3.27	0.02	0.006	0.55%	63.37	0.13	0.028	-0.20%	12.75	0.05	0.009	1.94%	0.14

2.10. Aluminum-Composite PLA (APLA)

**Figure 18.** APLA specimen set for one replication of measurements

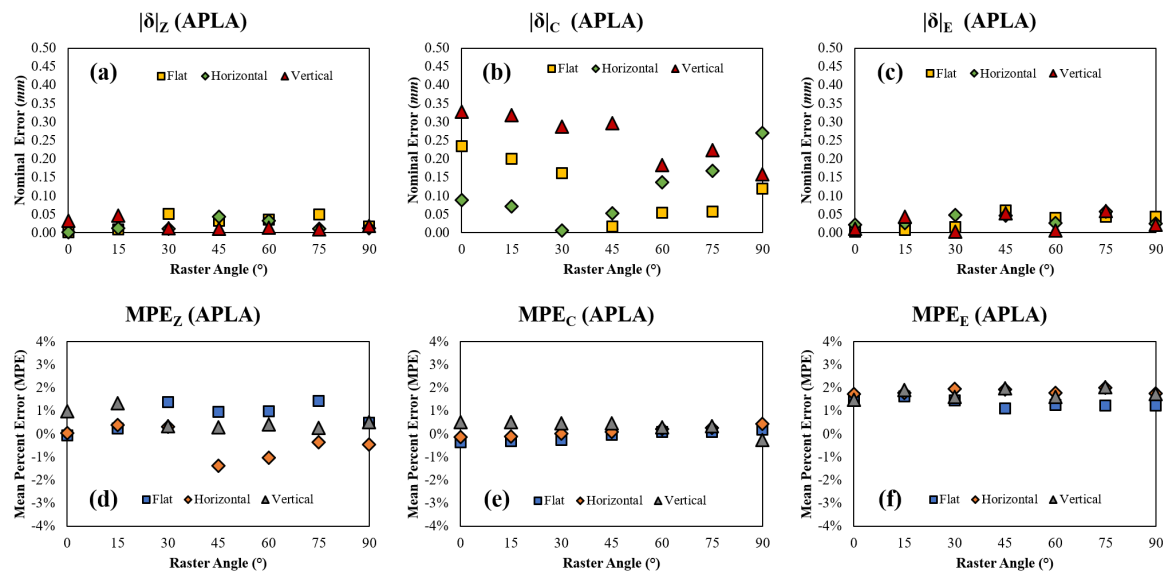


Figure 19. APLA (a) nominal error in Z, (b) nominal error in C, (c) nominal error in E, (d) mean percent error in Z, (e) mean percent error in C, and (f) mean percent error in E with respect to raster angle and orientation

Table 9. Mean, $|\delta|$, SE, MPE, and $|\Delta|$ for APLA as a function of print orientation and raster angle

Material: APLA (all dimensions in *mm* unless otherwise specified)

PO	Angle	Z (<i>n</i> = 10)				C (<i>n</i> = 10)				E (<i>n</i> = 10)				$ \Delta $
		μ	$ \delta $	SE	MPE	μ	$ \delta $	SE	MPE	μ	$ \delta $	SE	MPE	
F	0°	3.25	0.00	0.021	-0.07%	63.27	0.23	0.034	-0.37%	12.70	0.00	0.019	1.55%	0.23
F	15°	3.26	0.01	0.023	0.23%	63.30	0.20	0.031	-0.32%	12.71	0.01	0.028	1.62%	0.20
F	30°	3.30	0.05	0.047	1.37%	63.34	0.16	0.027	-0.25%	12.68	0.02	0.025	1.45%	0.17
F	45°	3.28	0.03	0.023	0.96%	63.48	0.02	0.034	-0.03%	12.64	0.06	0.029	1.10%	0.07
F	60°	3.29	0.04	0.032	0.98%	63.56	0.06	0.034	0.09%	12.66	0.04	0.032	1.25%	0.08
F	75°	3.30	0.05	0.031	1.43%	63.56	0.06	0.019	0.09%	12.66	0.04	0.029	1.23%	0.09
F	90°	3.27	0.02	0.023	0.48%	63.62	0.12	0.039	0.19%	12.66	0.04	0.030	1.23%	0.13
H	0°	3.25	0.00	0.013	0.05%	63.41	0.09	0.021	-0.14%	12.72	0.02	0.020	1.74%	0.09
H	15°	3.26	0.01	0.013	0.38%	63.43	0.07	0.013	-0.11%	12.73	0.03	0.020	1.78%	0.08
H	30°	3.26	0.01	0.013	0.32%	63.51	0.01	0.016	0.01%	12.75	0.05	0.026	1.94%	0.05
H	45°	3.21	0.04	0.018	-1.37%	63.55	0.05	0.017	0.08%	12.75	0.05	0.035	1.92%	0.08
H	60°	3.22	0.03	0.022	-1.04%	63.64	0.14	0.022	0.22%	12.73	0.03	0.018	1.78%	0.14
H	75°	3.24	0.01	0.016	-0.36%	63.67	0.17	0.029	0.26%	12.76	0.06	0.030	2.01%	0.18
H	90°	3.24	0.01	0.027	-0.46%	63.77	0.27	0.022	0.42%	12.72	0.02	0.025	1.76%	0.27
V	0°	3.28	0.03	0.016	0.98%	63.83	0.33	0.032	0.51%	12.69	0.01	0.024	1.49%	0.33
V	15°	3.30	0.05	0.032	1.34%	63.82	0.32	0.062	0.50%	12.74	0.04	0.036	1.90%	0.33
V	30°	3.26	0.01	0.020	0.33%	63.79	0.29	0.040	0.45%	12.70	0.00	0.027	1.59%	0.29
V	45°	3.26	0.01	0.022	0.29%	63.80	0.30	0.041	0.47%	12.75	0.05	0.028	1.98%	0.30
V	60°	3.26	0.01	0.019	0.40%	63.68	0.18	0.097	0.29%	12.71	0.01	0.036	1.61%	0.18
V	75°	3.26	0.01	0.022	0.26%	63.72	0.22	0.083	0.35%	12.76	0.06	0.030	2.03%	0.23
V	90°	3.27	0.02	0.021	0.51%	63.34	0.16	0.081	-0.25%	12.72	0.02	0.034	1.73%	0.16

2.11. Copper-Composite PLA (CPLA)

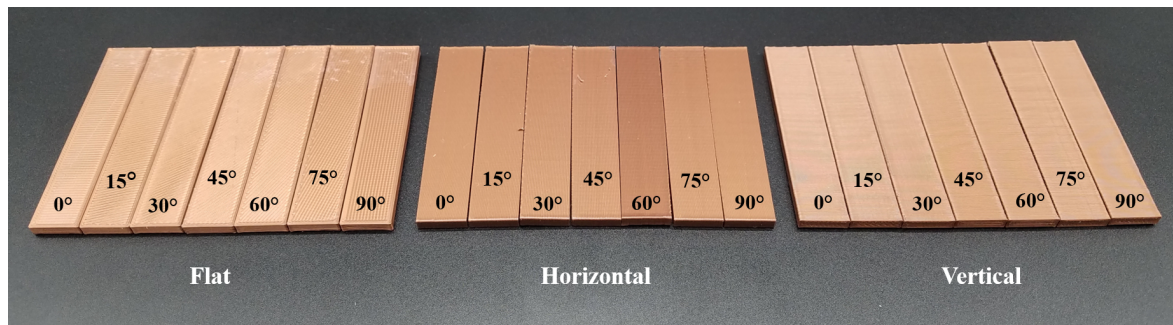


Figure 20. CPLA specimen set for one replication of measurements

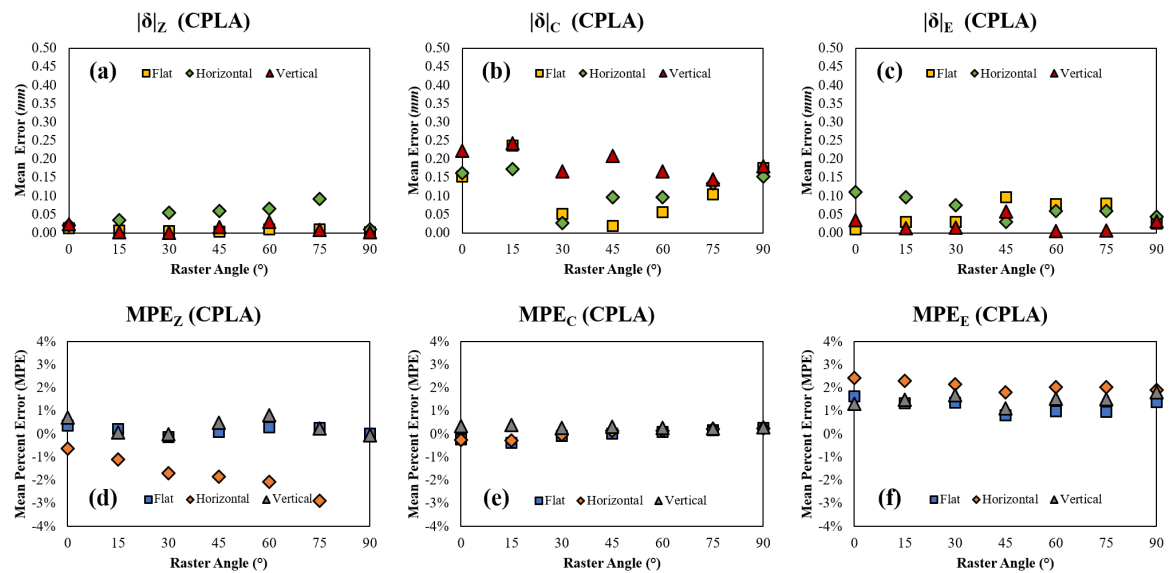


Figure 21. CPLA (a) nominal error in Z, (b) nominal error in C, (c) nominal error in E, (d) mean percent error in Z, (e) mean percent error in C, and (f) mean percent error in E with respect to raster angle and orientation

Table 10. Mean, $|\delta|$, SE, MPE, and $|\Delta|$ for CPLA as a function of print orientation and raster angle

Material: CPLA (all dimensions in mm unless otherwise specified)														
PO	Angle	Z (n = 10)				C (n = 10)				E (n = 10)				$ \Delta $
		μ	$ \delta $	SE	MPE	μ	$ \delta $	SE	MPE	μ	$ \delta $	SE	MPE	
F	0°	3.26	0.01	0.006	0.37%	63.35	0.15	0.024	-0.24%	12.71	0.01	0.018	1.64%	0.15
F	15°	3.26	0.01	0.006	0.21%	63.26	0.24	0.017	-0.37%	12.67	0.03	0.015	1.34%	0.24
F	30°	3.25	0.00	0.013	-0.14%	63.45	0.05	0.016	-0.08%	12.67	0.03	0.014	1.35%	0.06
F	45°	3.25	0.00	0.010	0.08%	63.52	0.02	0.009	0.03%	12.60	0.10	0.017	0.82%	0.10
F	60°	3.26	0.01	0.009	0.30%	63.56	0.06	0.010	0.09%	12.62	0.08	0.011	0.97%	0.10
F	75°	3.26	0.01	0.008	0.27%	63.60	0.10	0.016	0.16%	12.62	0.08	0.011	0.96%	0.13
F	90°	3.25	0.00	0.007	0.03%	63.68	0.17	0.021	0.27%	12.68	0.03	0.016	1.38%	0.18
H	0°	3.23	0.02	0.010	-0.63%	63.34	0.16	0.019	-0.26%	12.81	0.11	0.008	2.42%	0.20

H	15°	3.22	0.04	0.010	-1.10%	63.33	0.17	0.022	-0.27%	12.80	0.10	0.011	2.31%	0.20
H	30°	3.20	0.05	0.010	-1.70%	63.47	0.03	0.020	-0.04%	12.78	0.08	0.015	2.15%	0.10
H	45°	3.19	0.06	0.007	-1.85%	63.60	0.10	0.027	0.15%	12.73	0.03	0.008	1.80%	0.12
H	60°	3.18	0.07	0.010	-2.08%	63.60	0.10	0.024	0.15%	12.76	0.06	0.008	2.03%	0.13
H	75°	3.16	0.09	0.007	-2.88%	63.63	0.13	0.025	0.21%	12.76	0.06	0.011	2.03%	0.17
H	90°	3.26	0.01	0.008	0.27%	63.65	0.15	0.023	0.24%	12.74	0.04	0.012	1.91%	0.16
V	0°	3.27	0.02	0.010	0.72%	63.72	0.22	0.023	0.35%	12.67	0.03	0.010	1.31%	0.23
V	15°	3.25	0.00	0.004	0.06%	63.74	0.24	0.022	0.38%	12.69	0.01	0.013	1.48%	0.24
V	30°	3.25	0.00	0.007	0.00%	63.67	0.17	0.024	0.26%	12.71	0.01	0.007	1.68%	0.17
V	45°	3.27	0.02	0.005	0.49%	63.71	0.21	0.017	0.33%	12.64	0.06	0.014	1.12%	0.22
V	60°	3.28	0.03	0.030	0.81%	63.67	0.17	0.020	0.26%	12.70	0.00	0.012	1.54%	0.17
V	75°	3.26	0.01	0.006	0.24%	63.65	0.15	0.024	0.23%	12.69	0.01	0.015	1.52%	0.15
V	90°	3.25	0.00	0.008	-0.07%	63.68	0.18	0.013	0.28%	12.73	0.03	0.009	1.81%	0.18

2.12. Wood-Composite PLA (WPLA)

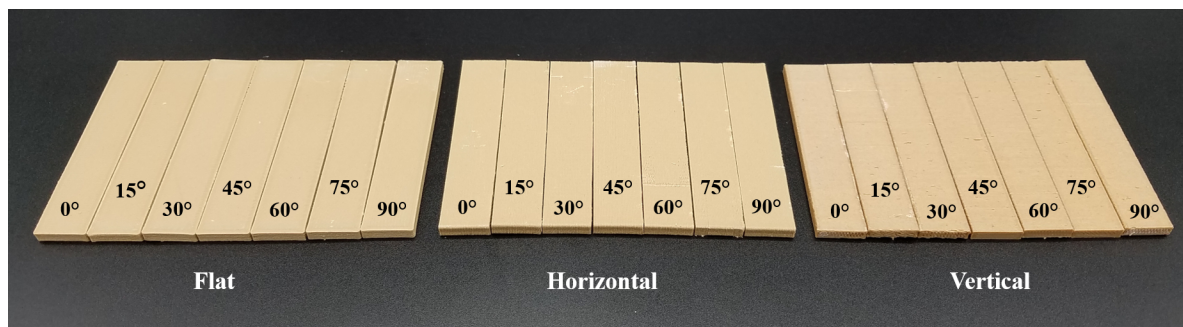


Figure 22. WPLA specimen set for one replication of measurements

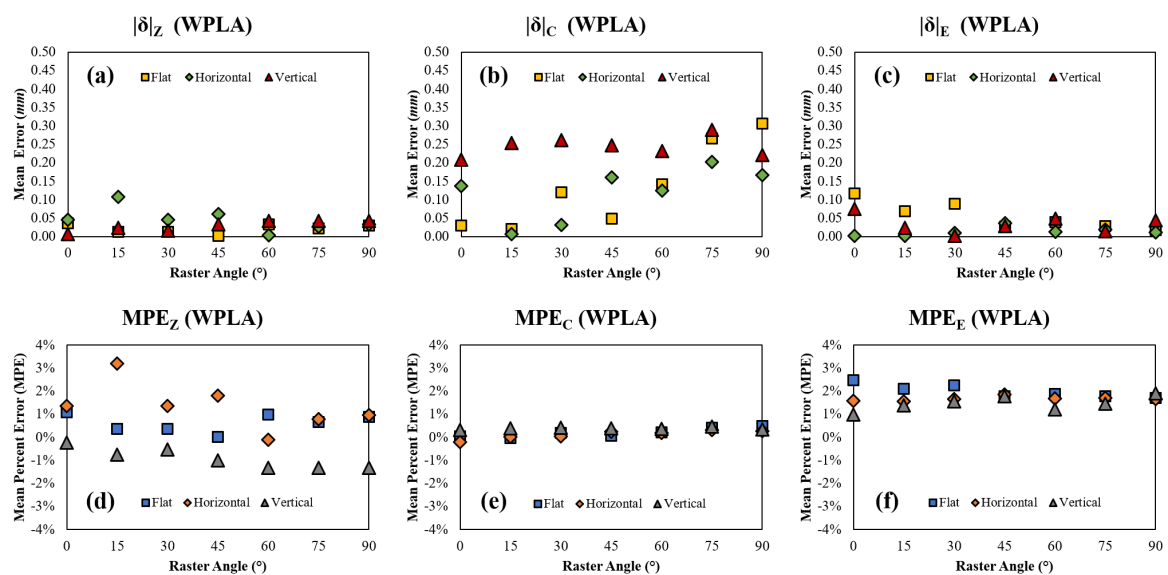


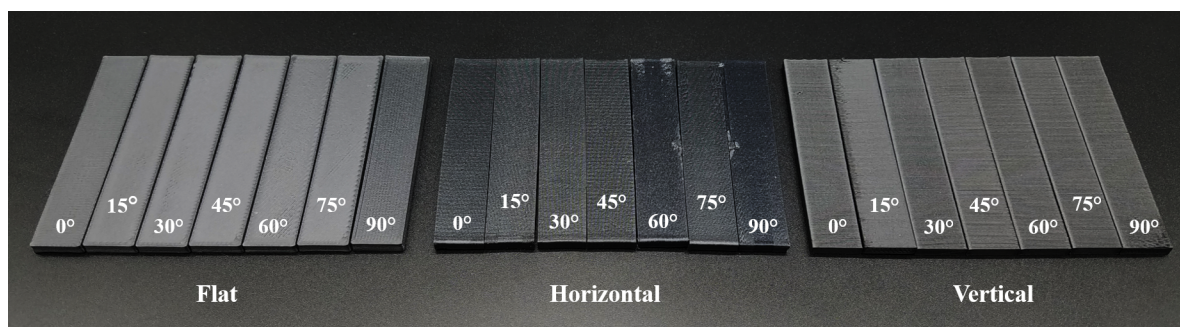
Figure 23. WPLA (a) nominal error in Z, (b) nominal error in C, (c) nominal error in E, (d) mean percent error in Z, (e) mean percent error in C, and (f) mean percent error in E with respect to raster angle and orientation

Table 11. Mean, $|\delta|$, SE, MPE, and $|\Delta|$ for WPLA as a function of print orientation and raster angle

Material: WPLA (all dimensions in mm unless otherwise specified)

PO	Angle	Z ($n = 10$)				C ($n = 10$)				E ($n = 10$)				$ \Delta $
		μ	$ \delta $	SE	MPE	μ	$ \delta $	SE	MPE	μ	$ \delta $	SE	MPE	
F	0°	3.29	0.04	0.014	1.08%	63.53	0.03	0.007	0.05%	12.82	0.12	0.016	2.47%	0.13
F	15°	3.26	0.01	0.009	0.36%	63.48	0.02	0.030	-0.03%	12.77	0.07	0.034	2.09%	0.07
F	30°	3.26	0.01	0.009	0.36%	63.62	0.12	0.017	0.19%	12.79	0.09	0.020	2.25%	0.15
F	45°	3.25	0.00	0.015	0.01%	63.55	0.05	0.022	0.08%	12.73	0.03	0.014	1.78%	0.06
F	60°	3.28	0.03	0.010	1.00%	63.64	0.14	0.020	0.22%	12.74	0.04	0.017	1.87%	0.15
F	75°	3.27	0.02	0.012	0.66%	63.77	0.27	0.021	0.42%	12.73	0.03	0.016	1.79%	0.27
F	90°	3.28	0.03	0.014	0.90%	63.81	0.31	0.018	0.48%	12.72	0.02	0.010	1.71%	0.31
H	0°	3.30	0.04	0.013	1.35%	63.36	0.14	0.052	-0.22%	12.70	0.00	0.021	1.58%	0.14
H	15°	3.36	0.11	0.014	3.20%	63.51	0.01	0.043	0.01%	12.70	0.00	0.022	1.56%	0.11
H	30°	3.30	0.04	0.010	1.36%	63.53	0.03	0.025	0.05%	12.71	0.01	0.028	1.65%	0.06
H	45°	3.31	0.06	0.013	1.80%	63.66	0.16	0.034	0.25%	12.74	0.04	0.025	1.85%	0.17
H	60°	3.25	0.00	0.015	-0.11%	63.63	0.13	0.049	0.20%	12.71	0.01	0.017	1.67%	0.13
H	75°	3.28	0.03	0.012	0.78%	63.70	0.20	0.041	0.32%	12.72	0.02	0.017	1.71%	0.20
H	90°	3.28	0.03	0.013	0.96%	63.67	0.17	0.028	0.26%	12.71	0.01	0.019	1.66%	0.17
V	0°	3.24	0.01	0.008	-0.22%	63.71	0.21	0.021	0.33%	12.63	0.07	0.014	0.99%	0.22
V	15°	3.23	0.02	0.011	-0.75%	63.75	0.25	0.025	0.40%	12.68	0.02	0.015	1.39%	0.26
V	30°	3.23	0.02	0.019	-0.53%	63.76	0.26	0.020	0.41%	12.70	0.00	0.019	1.57%	0.26
V	45°	3.22	0.03	0.008	-1.00%	63.75	0.25	0.015	0.39%	12.73	0.03	0.018	1.79%	0.25
V	60°	3.21	0.04	0.013	-1.32%	63.73	0.23	0.020	0.36%	12.65	0.05	0.018	1.20%	0.24
V	75°	3.21	0.04	0.010	-1.32%	63.79	0.29	0.025	0.45%	12.69	0.01	0.014	1.47%	0.29
V	90°	3.21	0.04	0.017	-1.34%	63.72	0.22	0.015	0.35%	12.74	0.04	0.017	1.91%	0.23

2.13. Carbon-Fiber-Composite PLA (CFPLA)

**Figure 24.** CFPLA specimen set for one replication of measurements

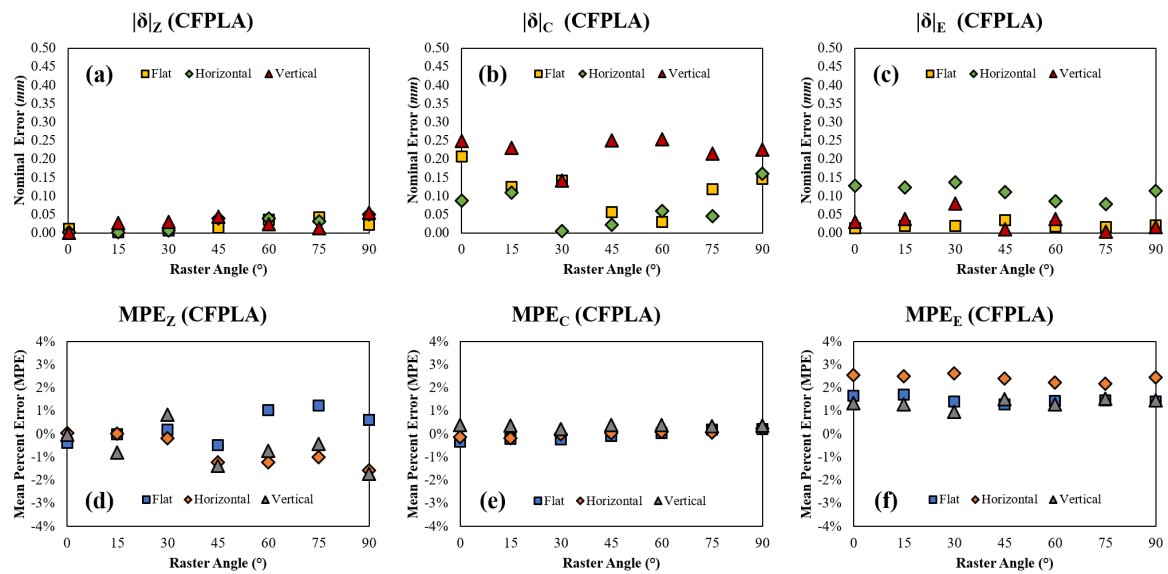


Figure 25. CFPLA (a) nominal error in Z, (b) nominal error in C, (c) nominal error in E, (d) mean percent error in Z, (e) mean percent error in C, and (f) mean percent error in E with respect to raster angle and orientation

Table 12. Mean, $|\delta|$, SE, MPE, and $|\Delta|$ for CFPLA as a function of print orientation and raster angle

Material: CFPLA (all dimensions in mm unless otherwise specified)

PO	Angle	$Z (n = 10)$				$C (n = 10)$				$E (n = 10)$				$ \Delta $
		μ	$ \delta $	SE	MPE	μ	$ \delta $	SE	MPE	μ	$ \delta $	SE	MPE	
F	0°	3.24	0.01	0.019	-0.37%	63.29	0.21	0.035	-0.33%	12.71	0.01	0.016	1.67%	0.21
F	15°	3.25	0.00	0.022	-0.01%	63.38	0.13	0.028	-0.20%	12.72	0.02	0.024	1.72%	0.13
F	30°	3.26	0.01	0.019	0.19%	63.36	0.14	0.033	-0.22%	12.68	0.02	0.035	1.42%	0.14
F	45°	3.24	0.01	0.020	-0.47%	63.44	0.06	0.022	-0.09%	12.67	0.03	0.044	1.29%	0.07
F	60°	3.29	0.04	0.025	1.04%	63.53	0.03	0.033	0.05%	12.68	0.02	0.027	1.44%	0.05
F	75°	3.29	0.04	0.025	1.22%	63.62	0.12	0.020	0.19%	12.68	0.02	0.020	1.45%	0.13
F	90°	3.27	0.02	0.028	0.61%	63.65	0.15	0.025	0.23%	12.68	0.02	0.021	1.42%	0.15
H	0°	3.25	0.00	0.015	0.04%	63.41	0.09	0.032	-0.14%	12.83	0.13	0.035	2.54%	0.15
H	15°	3.25	0.00	0.011	0.02%	63.39	0.11	0.030	-0.17%	12.82	0.12	0.031	2.51%	0.16
H	30°	3.24	0.01	0.007	-0.19%	63.50	0.01	0.025	-0.01%	12.84	0.14	0.025	2.62%	0.14
H	45°	3.21	0.04	0.008	-1.22%	63.52	0.02	0.048	0.03%	12.81	0.11	0.031	2.41%	0.12
H	60°	3.21	0.04	0.012	-1.23%	63.56	0.06	0.045	0.09%	12.79	0.09	0.026	2.23%	0.11
H	75°	3.22	0.03	0.008	-1.00%	63.55	0.05	0.048	0.07%	12.78	0.08	0.028	2.17%	0.10
H	90°	3.20	0.05	0.007	-1.57%	63.66	0.16	0.042	0.25%	12.81	0.11	0.030	2.45%	0.20
V	0°	3.25	0.00	0.017	-0.03%	63.75	0.25	0.053	0.39%	12.67	0.03	0.018	1.35%	0.25
V	15°	3.22	0.03	0.008	-0.81%	63.73	0.23	0.040	0.36%	12.66	0.04	0.021	1.28%	0.23
V	30°	3.28	0.03	0.023	0.84%	63.64	0.14	0.088	0.22%	12.62	0.08	0.019	0.96%	0.16
V	45°	3.21	0.04	0.011	-1.38%	63.75	0.25	0.037	0.39%	12.69	0.01	0.019	1.50%	0.25
V	60°	3.23	0.02	0.016	-0.73%	63.75	0.25	0.039	0.40%	12.66	0.04	0.024	1.28%	0.26
V	75°	3.24	0.01	0.020	-0.44%	63.72	0.21	0.052	0.34%	12.70	0.00	0.013	1.54%	0.22
V	90°	3.20	0.05	0.017	-1.72%	63.73	0.23	0.036	0.35%	12.68	0.02	0.017	1.45%	0.23

3. Methods

3.1. Choice of Materials

The set of materials chosen for this study is given in Table 1 in Section 2. This is not an exhaustive set of materials that can be processed using FDM, but these are the most common "hard" polymer materials used. Note that all materials used were available open-source and were not proprietary blends; this was done to ensure that the composition of the material was known and that manufacturer infill and additives were not used. Two other materials were examined during initial setup of the experiment (polyvinyl alcohol (PVA), thermoplastic polyurethane (TPU)) but these were found to be too soft and flexible after printing to accurately be measured. Each of the materials in the set were chosen specifically, the main reasons being:

- **ABS and PLA:** These are the most common FDM materials and therefore were the first two selected
- **HTPLA:** Standard PLA is quite sensitive to printing temperature and can be strengthened by printing at a higher temperature. However, standard PLA begins to burn and break down at a relatively low temperature above its melting point. Recently, high-temperature versions of the material have been in development; this has not been characterized in the literature yet, but the material appears to be about 20% tougher than standard PLA. It was selected because this authors believe it will become more widely used.
- **HIPS:** HIPS is a common construction material when molded; its primary use in AM is in the printing of support material. However, the authors have successfully used it as a standard AM material and it appears to have properties similar to ABS but with much less tendency to shrink and warp on cooling. It is a useful, if not common, material for FDM and was therefore included in the set.
- **Nylon, PETG, and PC:** These are becoming very common FDM materials, overtaking ABS and PLA for some applications. They are stronger and generally more stable for many uses, particularly those involving fracture and fatigue. They are standard materials that should be included in every large dataset for this reason.
- **Composite PLAs:** As the use of PLA expands, particularly in green production and medical devices, ways to improve its properties have been a topic of much recent research. There are a large number of composite PLAs available, and a subset of four that have different types of composite infill were selected for testing. The authors were particularly interested in metal-powder PLA (5% (CPLA) and 40% (APLA)), in soft material infill (WPLA), and in chopped fiber infill (CFPLA) cases.

3.2. Setup and Printing Parameters

The printing parameters for each of the materials are shown in Table 13 below. The authors are very experienced using all of these materials and so used standard print settings for these materials. The settings recommended by the filament manufacturers were used at first and these adjusted to produce the best combination of part quality and print speed. Note that these settings were developed over hundreds of parts for each material, so they are known to work well and produce the best possible results for each material used. The samples were printed in batches (Figure X) to ensure that the minimal residual error possible was present and that all significant error observed came from material behavior and the mechanical behavior of the printers.

As previously noted, some of the materials required a tool steel nozzle for processing due to flow and abrasion problems with the material. The PLA-based materials in particular needed this type of extruder. Some materials were also printed inside of an enclosure. Two different printers were used for this study, an open-bed Prusa-frame machine built and tuned by the authors and a modified XYZPrinting DaVinci Pro 1.0 machine that used open-source filament and software to pre-process

the materials. The pre-processing software used was Ultimaker Cura for the open-bed printer and an open-source version of XYZWare Pro for the DaVinci printer; both allowed complete control of the printing parameters shown in Table 13. All layer thicknesses were set at 200 μm for all samples; appropriate filament retraction settings were used to both avoid messy extruder and to avoid gaps and voids in the part infill. Rafts were used as well to ensure that the printing surface itself did not introduce error into the measurements. The Prusa-frame machine used a heated aluminum-polycarbonate build plate [27] and the DaVinci machine used a heated aluminum-glass build plate as a base. Tests were run on both printers before making the samples to ensure that the extruders and build plates were producing the correct temperatures; both a type-K thermocouple reader and a infrared thermometer were used.

Table 13. Specimen manufacturing parameters

Material	Velocity (mm/s)	Jerk (mm/s)	$T_{extruder}$ ($^{\circ}C$)	$T_{printbed}$ ($^{\circ}C$)	Nozzle Type	Environment
ABS	50	8	225	90	0.4 mm Brass	Enclosed
PLA	60	8	200	50	0.4 mm Steel	Open
HTPLA	60	8	245	50	0.4 mm Steel	Open
HIPS	60	8	240	90	0.4 mm Brass	Enclosed
Nylon	50	8	250	70	0.4 mm Brass	Enclosed
PETG	60	8	240	80	0.4 mm Steel	Open
PC	30	8	260	90	0.4 mm Brass	Enclosed
APLA	60	8	200	50	0.4 mm Steel	Open
CPLA	60	8	205	50	0.4 mm Steel	Open
WPLA	60	8	210	50	0.4 mm Steel	Open
CFPLA	40	8	200	50	0.4mm Steel	Open

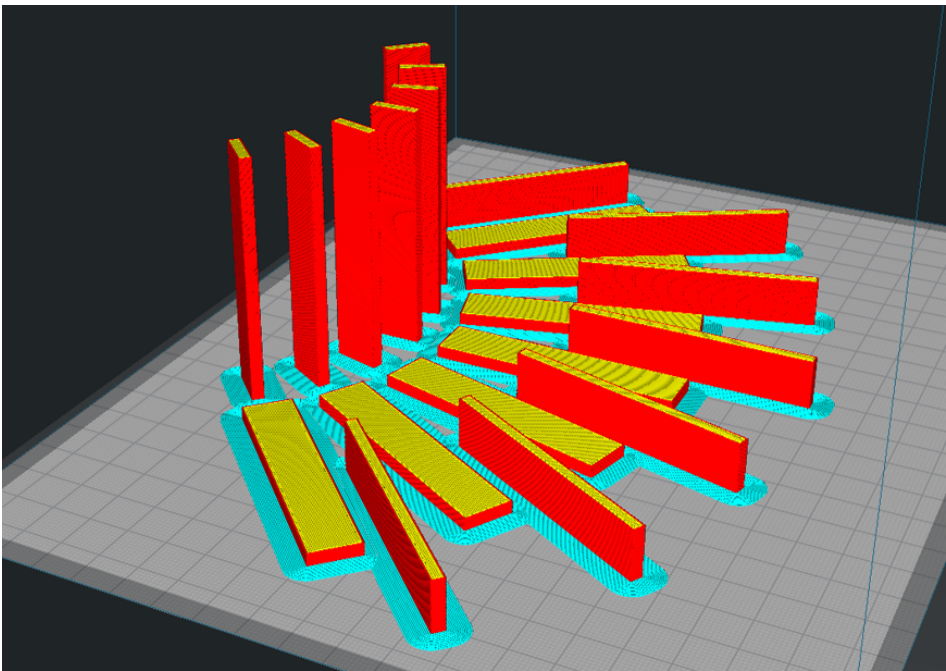


Figure 26. Pre-processed batch of samples showing orientation, angle, and raft and layer settings; note the shell (red) and the infill (yellow) regions in the parts for the different orientations

3.3. Data Collection

Since the purpose of this study was to collect a large dataset on the overall dimensional accuracy and repeatability for FDM, the measurement of complex features and surface roughness were not needed. Therefore, the measurement process was very simple: all measurements were made using a set of good quality vernier calipers with a resolution of 1/100 mm, as shown in Figure 27 below.

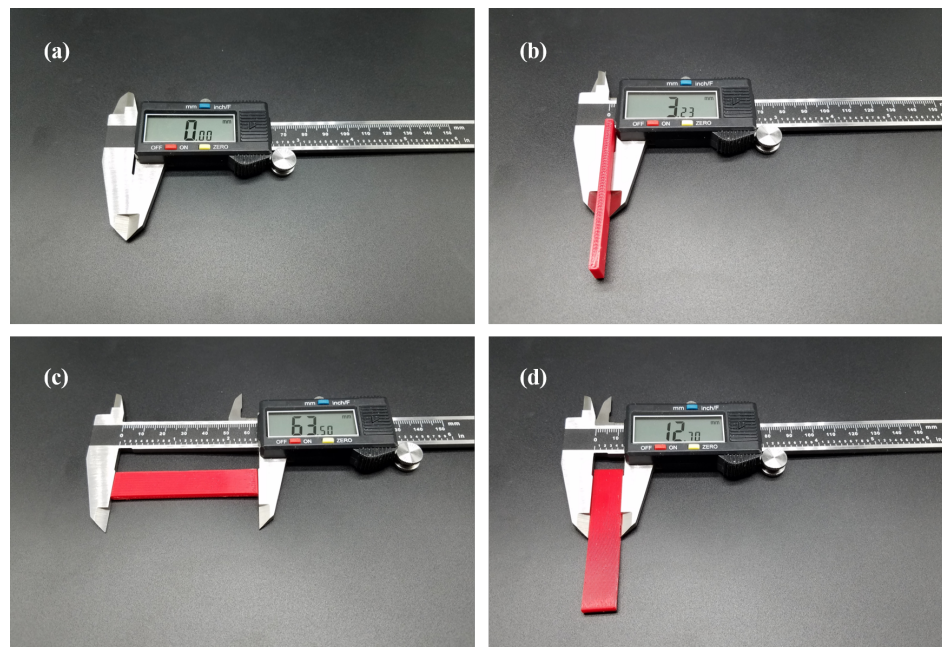


Figure 27. Vernier calipers for measurement (a) tared before using, (b) measuring *Z*, (c) measuring *C*, and (d) measuring *E*

All samples were checked before measurement and any clearly defective samples discarded from the set. These defects were very rare, however, with only seven defective (and replaced) specimens observed from a population of over 2000 samples.

Supplementary Materials: Please fill in after posting the dataset with the manuscript

Author Contributions: TRP, AEP, and SLM conceived the idea for the dataset, TRP and AEP collected the data, ML, AEP, and FOD helped to organize and interpret the data and do the basic statistical analysis, FOD and SLM provided supervision and advice on the project, TRP and AEP manufactured the specimens, and SLM provided raw materials. All authors assisted with writing and revising the manuscript. Author order was agreed by all authors prior to manuscript submission.

Funding: This work received no external funding

Conflicts of Interest: The authors declare no conflict of interest. No external funding was used to perform the work described in this study. Opinions and conclusions presented in this work are solely those of the authors.

References

1. Gibson, I.; Rosen, D.; Stucker, B. *Additive Manufacturing Technologies: 3D Printing, Rapid Prototyping, and Direct Digital Manufacturing*; Springer, 2016.
2. Guo, N.; Leu, M.C. Additive manufacturing: technology, applications and research needs. *Frontiers of Mechanical Engineering* **2013**, *8*, 215–243. doi:10.1007/s11465-013-0248-8.
3. ASTM. F2792-12a: Standard Terminology for Additive Manufacturing Technologies. *ASTM Standard (Withdrawn)* **2012**. doi:10.1520/f2792-12a.

4. Yang, S.; Zhao, Y.F. Additive manufacturing-enabled design theory and methodology: a critical review. *The International Journal of Advanced Manufacturing Technology* **2015**, *80*, 327–342. doi:10.1007/s00170-015-6994-5.
5. Yang, S.; Tang, Y.; Zhao, Y.F. A new part consolidation method to embrace the design freedom of additive manufacturing. *Journal of Manufacturing Processes* **2015**, *20*, 444–449. doi:10.1016/j.jmapro.2015.06.024.
6. Ford, S.; Despeisse, M. Additive manufacturing and sustainability: an exploratory study of the advantages and challenges. *Journal of Cleaner Production* **2016**, *137*, 1573–1587. doi:10.1016/j.jclepro.2016.04.150.
7. Tofail, S.A.; Koumoulos, E.P.; Bandyopadhyay, A.; Bose, S.; O'Donoghue, L.; Charitidis, C. Additive manufacturing: scientific and technological challenges, market uptake and opportunities. *Materials Today* **2018**, *21*, 22–37. doi:10.1016/j.mattod.2017.07.001.
8. Falck, R.; Goushegir, S.; dos Santos, J.; Amancio-Filho, S. AddJoining: A novel additive manufacturing approach for layered metal-polymer hybrid structures. *Materials Letters* **2018**, *217*, 211–214. doi:10.1016/j.matlet.2018.01.021.
9. Cunico, M.W.M.; de Carvalho, J. Development of additive manufacturing technology based on selective metal-polymer composite formation. *Rapid Prototyping Journal* **2018**, *24*, 52–68. doi:10.1108/rpj-12-2016-0200.
10. Khatri, B.; Lappe, K.; Noetzel, D.; Pursche, K.; Hanemann, T. A 3D-Printable Polymer-Metal Soft-Magnetic Functional Composite—Development and Characterization. *Materials* **2018**, *11*, 189. doi:10.3390/ma11020189.
11. Gonzalez-Gutierrez, J.; Cano, S.; Schuschnigg, S.; Kukla, C.; Sapkota, J.; Holzer, C. Additive Manufacturing of Metallic and Ceramic Components by the Material Extrusion of Highly-Filled Polymers: A Review and Future Perspectives. *Materials* **2018**, *11*, 840. doi:10.3390/ma11050840.
12. Silva, M.; Felismina, R.; Mateus, A.; Parreira, P.; Malça, C. Application of a Hybrid Additive Manufacturing Methodology to Produce a Metal/Polymer Customized Dental Implant. *Procedia Manufacturing* **2017**, *12*, 150–155. doi:10.1016/j.promfg.2017.08.019.
13. Lee, P.H.; Chung, H.; Lee, S.W.; Yoo, J.; Ko, J. Review: Dimensional Accuracy in Additive Manufacturing Processes. ASME 2014 International Manufacturing Science and Engineering Conference collocated with the JSME 2014 International Conference on Materials and Processing and the 42nd North American Manufacturing Research Conference, June 9-13, 2014, Detroit, Michigan, USA: V001T04A045. ASME, 2014. doi:10.1115/msec2014-4037.
14. Guessasma, S.; Zhang, W.; Zhu, J.; Belhabib, S.; Nouri, H. Challenges of additive manufacturing technologies from an optimisation perspective. *International Journal for Simulation and Multidisciplinary Design Optimization* **2015**, *6*, A9. doi:10.1051/smdo/2016001.
15. Kirsch, K.L.; Snyder, J.C.; Stimpson, C.K.; Thole, K.A.; Mongillo, D. Repeatability in Performance of Micro Cooling Geometries Manufactured with Laser Powder Bed Fusion. 53rd AIAA/SAE/ASEE Joint Propulsion Conference. American Institute of Aeronautics and Astronautics, 2017. doi:10.2514/6.2017-4706.
16. Rebaioli, L.; Fassi, I. A review on benchmark artifacts for evaluating the geometrical performance of additive manufacturing processes. *The International Journal of Advanced Manufacturing Technology* **2017**, *93*, 2571–2598. doi:10.1007/s00170-017-0570-0.
17. Zongo, F.; Tahan, A.; Aidibe, A.; Brailovski, V. Intra- and Inter-Repeatability of Profile Deviations of an AlSi10Mg Tooling Component Manufactured by Laser Powder Bed Fusion. *Journal of Manufacturing and Materials Processing* **2018**, *2*, 56. doi:10.3390/jmmp2030056.
18. Taheri, H.; Shoaib, M.R.B.M.; Koester, L.W.; Bigelow, T.A.; Collins, P.C.; Bond, L.J. Powder-based additive manufacturing - a review of types of defects, generation mechanisms, detection, property evaluation and metrology. *International Journal of Additive and Subtractive Materials Manufacturing* **2017**, *1*, 172. doi:10.1504/ijasm.2017.088204.

19. Günther, J.; Brenne, F.; Droste, M.; Wendler, M.; Volkova, O.; Biermann, H.; Niendorf, T. Design of novel materials for additive manufacturing - Isotropic microstructure and high defect tolerance. *Scientific Reports* **2018**, *8*. doi:10.1038/s41598-018-19376-0.
20. Gordeev, E.G.; Galushko, A.S.; Ananikov, V.P. Improvement of quality of 3D printed objects by elimination of microscopic structural defects in fused deposition modeling. *PLOS ONE* **2018**, *13*, e0198370. doi:10.1371/journal.pone.0198370.
21. Dimitrov, D.; van Wijck, W.; Schreve, K.; de Beer, N. Investigating the achievable accuracy of three dimensional printing. *Rapid Prototyping Journal* **2006**, *12*, 42–52. doi:10.1108/13552540610637264.
22. Yaman, U. Shrinkage compensation of holes via shrinkage of interior structure in FDM process. *The International Journal of Advanced Manufacturing Technology* **2017**, *94*, 2187–2197. doi:10.1007/s00170-017-1018-2.
23. Schmutzler, C.; Zimmermann, A.; Zaeh, M.F. Compensating Warpage of 3D Printed Parts Using Free-form Deformation. *Procedia CIRP* **2016**, *41*, 1017–1022. doi:10.1016/j.procir.2015.12.078.
24. Agrawal, S.; Dhande, S.G. Analysis of mechanical error in a fused deposition process using a stochastic approach. *International Journal of Production Research* **2007**, *45*, 3991–4012. doi:10.1080/00207540600791624.
25. Bochmann, L.; Bayley, C.; Helu, M.; Transchel, R.; Wegener, K.; Dornfeld, D. Understanding error generation in fused deposition modeling. *Surface Topography: Metrology and Properties* **2015**, *3*, 014002. doi:10.1088/2051-672x/3/1/014002.
26. Lienenke, T.; Denzer, V.; Adam, G.A.; Zimmer, D. Dimensional Tolerances for Additive Manufacturing: Experimental Investigation for Fused Deposition Modeling. *Procedia CIRP* **2016**, *43*, 286–291. doi:10.1016/j.procir.2016.02.361.
27. Messimer, S.L.; Patterson, A.E.; Muna, N.; Deshpande, A.P.; Pereira, T.R. Characterization and Processing Behavior of Heated Aluminum-Polycarbonate Composite Build Plates for the FDM Additive Manufacturing Process. *Journal of Manufacturing and Materials Processing* **2018**, *2*, 12. doi:10.3390/jmmp2010012.
28. Turner, B.N.; Strong, R.; Gold, S.A. A review of melt extrusion additive manufacturing processes: I. Process design and modeling. *Rapid Prototyping Journal* **2014**, *20*, 192–204. doi:10.1108/rpj-01-2013-0012.
29. Turner, B.N.; Gold, S.A. A review of melt extrusion additive manufacturing processes: II. Materials, dimensional accuracy, and surface roughness. *Rapid Prototyping Journal* **2015**, *21*, 250–261. doi:10.1108/rpj-02-2013-0017.
30. Mohamed, O.A.; Masood, S.H.; Bhowmik, J.L. Optimization of fused deposition modeling process parameters: a review of current research and future prospects. *Advances in Manufacturing* **2015**, *3*, 42–53. doi:10.1007/s40436-014-0097-7.
31. Mohamed, O.; Masood, S.; Bhowmik, J. Analytical Modelling and Optimization of the Temperature-Dependent Dynamic Mechanical Properties of Fused Deposition Fabricated Parts Made of PC-ABS. *Materials* **2016**, *9*, 895. doi:10.3390/ma9110895.
32. Sood, A.K.; Ohdar, R.; Mahapatra, S. Parametric appraisal of mechanical property of fused deposition modelling processed parts. *Materials & Design* **2010**, *31*, 287–295. doi:10.1016/j.matdes.2009.06.016.
33. Chang, D.Y.; Huang, B.H. Studies on profile error and extruding aperture for the RP parts using the fused deposition modeling process. *The International Journal of Advanced Manufacturing Technology* **2010**, *53*, 1027–1037. doi:10.1007/s00170-010-2882-1.
34. Saqib, S.; Urbanic, J. An Experimental Study to Determine Geometric and Dimensional Accuracy Impact Factors for Fused Deposition Modelled Parts. In *Enabling Manufacturing Competitiveness and Economic Sustainability*; Springer Berlin Heidelberg, 2011; pp. 293–298. doi:10.1007/978-3-642-23860-4_48.
35. Sood, A.K.; Ohdar, R.; Mahapatra, S. Improving dimensional accuracy of Fused Deposition Modelling processed part using grey Taguchi method. *Materials & Design* **2009**, *30*, 4243–4252. doi:10.1016/j.matdes.2009.04.030.

36. Sahu, R.K.; Mahapatra, S.; Sood, A.K. A Study on Dimensional Accuracy of Fused Deposition Modeling (FDM) Processed Parts using Fuzzy Logic. *Journal for Manufacturing Science & Production* **2013**, *13*. doi:10.1515/jmsp-2013-0010.
37. Equbal, A.; Sood, A.K.; Mahapatra, S. Prediction of dimensional accuracy in fused deposition modelling: a fuzzy logic approach. *International Journal of Productivity and Quality Management* **2011**, *7*, 22. doi:10.1504/ijpqm.2011.037730.
38. Pennington, R.C.; Hoekstra, N.L.; Newcomer, J.L. Significant factors in the dimensional accuracy of fused deposition modelling. *Proceedings of the Institution of Mechanical Engineers, Part E: Journal of Process Mechanical Engineering* **2005**, *219*, 89–92. doi:10.1243/095440805x6964.
39. Huynh, H.N.; Nguyen, A.T.; Ha, N.L.; Thai, T.T.H. Application of fuzzy Taguchi method to improve the dimensional accuracy of Fused Deposition Modeling processed product. 2017 International Conference on System Science and Engineering (ICSSE). IEEE, 2017. doi:10.1109/icsse.2017.8030847.
40. Pérez, C.J.L. Analysis of the surface roughness and dimensional accuracy capability of fused deposition modelling processes. *International Journal of Production Research* **2002**, *40*, 2865–2881. doi:10.1080/00207540210146099.
41. ASTM. ASTM D256-10e1: *Standard Test Methods for Determining the Izod Pendulum Impact Resistance of Plastics*; ASTM International, 2018.